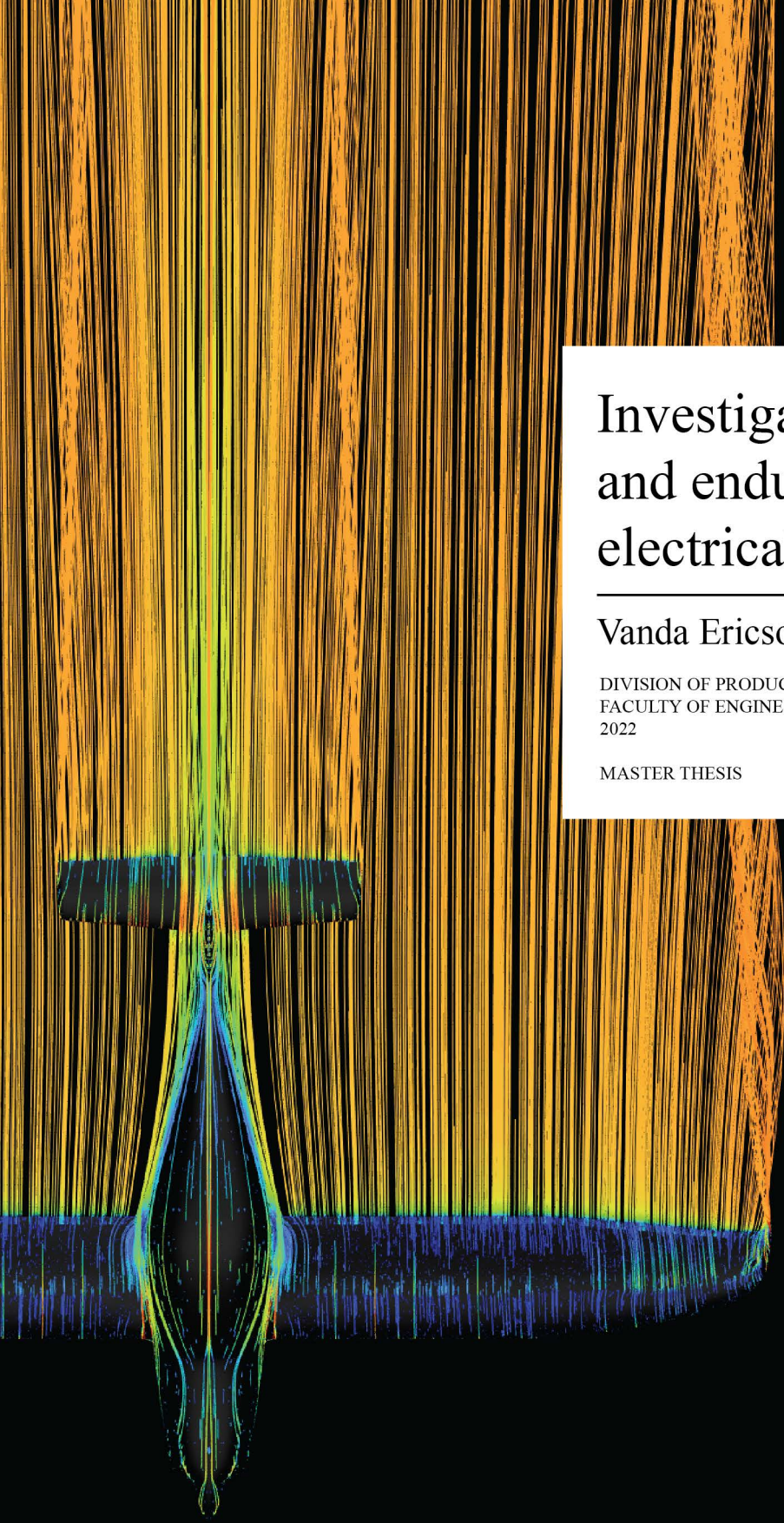

Investigation of the wing design and endurance of an ultralight electrical aircraft

Vanda Ericson & Jonathan Palmgren

DIVISION OF PRODUCT DEVELOPMENT | DEPARTMENT OF DESIGN SCIENCES
FACULTY OF ENGINEERING LTH | LUND UNIVERSITY
2022

MASTER THESIS

BLACKWING
SWEDEN

Investigation of the wing design and endurance of an ultralight electrical aircraft

Vanda Ericson and Jonathan Palmgren

LUND
UNIVERSITY

Investigation of the wing design and endurance of an ultralight electrical aircraft

Published by

Department of Design Sciences

Faculty of Engineering LTH, Lund University

P.O. Box 118, SE-221 00 Lund, Sweden

Subject: Product Development (MMKM05)

Division: Division of Product Development, Department of Design Sciences, Faculty of Engineering LTH, Lund University

Supervisor: Joze Tavcar & Johan Revstedt

Co-supervisor: Niklas Anderberg

Examiner: Axel Nordin

Abstract

The goal of this thesis was to explore the conversion of a propeller driven two-seater combustion airplane to an electrical airplane. Four different wing designs were considered. Two variations of Blackwing Sweden AB's current Blackwing wing (BW), a longer wing (BW-L) and a shorter wing (BW-S), as well as a new wing with a different airfoil (GW). Using Computational Fluid Dynamics the wings were modeled for different angles of attack to explore the aerodynamic properties. The range and endurance of the wings as well as the minimum and maximum velocities were analyzed.

The computational modeling was conducted with both the SST k-ω and the Transitional SST turbulence model. The transitional model takes the laminar boundary layer into account, providing a more accurate result, since the wing profiles are laminar. GW was found more sensitive to the turbulence model used, and it was deducted that it was less robust than the BW wings.

By varying the specific energy of the batteries in the airplane, the required energy needed to achieve the two hour flight target set by the company was explored. The airplane was compared to similar electric airplanes to analyze the market competitiveness.

The results concluded that GW had the best range and endurance, however the cost would be higher, since it would require new tools to be produced. The recommendation to the company is to continue with the wing that had the second best range and endurance, BW-L.

Keywords: Aerodynamics; Electrical Aviation; CFD; Endurance; Drag.

Sammanfattning

Målet med denna avhandling var att utforska omvandlingen av ett propellerdrivet tvåsitsigt förbränningsflygplan till ett elektriskt flygplan. Fyra olika vingdesigner övervägdes. Två varianter av Blackwing Sweden AB:s nuvarande Blackwing-vinge (BW), en längre vinge (BW-L) och en kortare vinge (BW-S), samt en ny vinge med annan vingprofil (GW). Med hjälp av beräkningsströmmningsmekanik modellerades vingarna för olika anfallsvinklar för att utforska de aerodynamiska egenskaperna. Vingarnas räckvidd och uthållighet samt minimi- och maximihastigheter analyserades.

Modelleringen utfördes både med turbulensmodellerna SST k-ω och Transitional SST. Transitionsmodellen tar hänsyn till det laminära gränsskiktet, vilket ger ett mer realistiskt resultat eftersom vingprofilerna är laminära. GW visade sig vara känsligare för den turbulensmodell som användes, och det konstaterades att den var mindre robust än BW-vingarna.

Genom att variera den specifika energin hos batterierna i flygplanet undersöktes den energi som krävdes för att uppnå det tvåtimmarsflygmål som företaget satt upp. Flygplanet jämfördes med liknande elektriska flygplan för att analysera konkurrenskraften på marknaden.

Från resultaten drogs slutsatsen att GW hade den bästa räckvidden och uthålligheten, men eftersom det skulle krävas nya verktyg för att producera vingen var kostnaderna högre. Den rekommenderade vingen är därmed den vingen med den näst bästa räckvidden och uthålligheten, BW-L.

Nyckelord: Aerodynamik; Eldrivet flygplan; CFD; Flygtid; Motståndskraft.

Acknowledgements

We would like to thank Niklas Anderberg of Blackwing Sweden AB for making this master thesis possible. Thank you for your guidance and patience.

We are extremely grateful towards Professor Johan Revstedt and Senior Lecture Joze Tavcar of Lund University for all the support and counseling that we received from you as our supervisors.

A big thanks to Robert-Zoltán Szász, Reasearcher at Lund University, for all the help with everything related to computers and software, without you we would still be looking for the terminal window.

A special thanks to Philip Månsson, Aeronautical Engineer at Saab, for providing us with knowledge and making our journey through this master thesis process easier.

Lund, May 2022

Vanda Ericson & Jonathan Palmgren

Table of Contents

List of Acronyms and Abbreviations

Acronyms and Abbreviations

AOA	Angle of Attack
BOI	Body of Influence
BW	BlackWing
BW-L	BlackWing Long
BW-S	BlackWing Short
CG	Center of Gravity
CFD	Computational Fluid Dynamics
GW	GreenWing
RANS	Reynolds Averaged Navier Stokes
SST	Shear Stress Transport

Nomenclature

α	Angle of Attack	$^\circ$
AR	Aspect Ratio	
a_h	Horizontal acceleration	m/s^2
a_v	Vertical acceleration	m/s^2
C_D	Coefficient of Drag	
C_{D_i}	Lift-induced drag coefficient	
$C_{D_{min}}$	Minimum drag coefficient	
C_L	Coefficient of Lift	
$C_{L_{E,max}}$	Coefficient of Lift at maximum endurance	
$C_{L_{minD}}$	Coefficient of Lift at minimum drag	
C_M	Pitching moment coefficient	
D	Drag Component	N
D_i	Lift-induced Drag Component	N
D_{min}	Minimum Drag Component	N
e	Oswald's span efficiency	
E	Endurance	s
$E_{battery}$	Battery Energy	Wh
E^*	Mass Specific Energy	Wh/kg
f	Equivalent flat plat area	m^2
g	Standard acceleration of gravity	N/kg
k	Lift-Induced drag constant	
LD_{max}	Maximum lift-to-drag ratio	
$m_{battery}$	Mass of Battery	kg
m	Mass of Airplane	kg
η_{total}	System Efficiency (from battery to propeller)	
η_p	Propeller efficiency	
$P_{aircraft}$	Propulsive Power	W
$P_{battery}$	Electric Power Provided From Battery	W
P_W	Engine Power	W
P_{REQ}	Power Required to preserve Level Flight	W
q_∞	Dynamic pressure	N/m^2
R	Range	m

R_e	Reynolds number	
S	Reference area of the wing	m^2
t	Time	s
T	Instantaneous Thrust	N
T_{AV}	Thrust Available	N
T_{REQ}	Thrust Required	N
V_∞	Far-field Airspeed	m/s
$V_{E_{max}}$	Airspeed of maximum endurance	m/s
$V_{LD_{max}}$	Airspeed of maximum lift-to-drag ratio	m/s
V_{max}	Maximum Airspeed	m/s
V_{min}	Minimum Airspeed	m/s
$V_{PR_{min}}$	Airspeed of minimum power required	m/s
$V_{R_{max}}$	Airspeed of maximum range	m/s
V_S	Stall airspeed	m/s
$V_{TR_{min}}$	Airspeed of minimum thrust required	m/s
W	Typical Weight of Airplane at condition	N
X_{tr}	Transition point with normalized chord	

1 Introduction

1.1 Background

The design of an aircraft is essential for the aircraft's performance, range and handling properties. The beauty of airplane design is that it requires multiple disciplines to join in perfect harmony to produce an airplane with the properties that best suit the intended mission [1]. Adding more fuel to an aircraft won't necessarily mean that the aircraft travels further, the whole aircraft is designed and built for a certain velocity at a certain height with a certain weight. Safety in aeronautics is of the highest importance, when the airplane is in the air, the only way is down, preferably in a controlled fashion.

1.1.1 The Electrical Propulsion System

The interest for electrical vehicles has grown considerably over the last years, this is no different in the aviation industry. Unlike for ground based vehicles, where the system mass is of relatively low importance, in aeronautics all systems are much more constrained by their weight. Due to this sensitivity to mass, an electrical aircraft was not feasible for many years, however, in 1940 Fred Militky began experimenting with electrical motors to propel model aircraft. The results he obtained were unsuccessful, the motors and batteries were too heavy. 20 years later, he successfully produced a small model airplane that was sold to the hobby market. In 1972 Ni-Cd batteries with higher power densities became available, with the new technology he aided in the modification of a HB-3 motor-glider that lead to the first electric flight of a manned aircraft in 1973. The flight was short, only 15 minutes, but it demonstrated the possibilities of electrical propulsion. [2]

Conventional combustion airplanes store the fuel in liquid form, during the flight the fuel is consumed and the mass of the airplane during flight is reduces, affecting the performance [2]. The reduction of fuel moves the center of gravity, CG, of the airplane, thus design decisions must be made with this in consideration [1]. This phenomena does not occur with electric batteries, making the design process in this

aspect easier.

Currently batteries have around a factor of 18 lower volume specific energy and a factor of 60 lower mass specific energy than kerosene. Existing batteries are even outperformed by 3.5% milk (although milk is yet to be able to function as airplane fuel) [2]. The mass specific energy leads to more mass of the aircraft in order to fly a sensible distance. The difference in mass leads to a different optimal cruise speed [3], thus leading to the need of design changes.

The biggest limitation with electrical aircrafts is the weight of the batteries. The current specific energy of batteries in is around 260 Wh/kg, however these batteries require cooling and in electric vehicles the specific energy is therefore reduced to around 150 Wh/kg [4]. The flight time and range of an aircraft is highly dependent on the amount of power available as well as the weight of the aircraft. The required specific energy of batteries for electric aircrafts depends on the design of the aircraft and on the intended take off weight. The battery capacity required for a commercial aircraft with over 100 passengers is higher than that required from an ultralight weight airplane that has two passengers.

1.1.2 Range and Endurance

An airplane is, in its simplest form, a transportation device. How this transportation is performed can be described by range and endurance. The range of an airplane is the total distance that can be travelled during one mission. The endurance measures how long the airplane can stay airborne, given a certain amount of fuel. Being able to predict range and endurance, for different flight cases and scenarios, is essential both in terms of efficiency and safety. [1]

The cruise stage is, of all the flight stages of a mission, arguably the most interesting stage when it comes to investigating range and endurance performance. By mapping the possible performance output of an airplane during cruise, several key parameters can be identified. [1]

When exploring the straight, level, and steady cruising phase of the flight mission, a lot can be revealed through drag and thrust modeling. There are several model proposals available when it comes to mapping the range and endurance performance, including models taking an electrical driven propeller into consideration. The challenge in creating an accurate model, mainly lies in the accuracy of the drag model. With the total drag consisting of several types of drag-inducing parameters, it is not uncommon to miss out, incorrectly neglect, or miscalculate, the total drag force. [1]

1.2 Project Background

Blackwing Sweden AB is a Swedish ultralight aircraft producer that have won multiple design awards. The company is now looking towards electrical aviation and have begun a project called GreenWing that aims to design, produce and flight test a wing specially made for electrical two seated school/travel airplanes with a flight time of two hours at 50 m/s.

The estimated flight time stems from the current capacity of batteries of 200 Wh/kg providing one hour airborne at 61 m/s for the GreenWing airplane. According to Blackwing Sweden AB more powerful and lightweight batteries are not far away, providing more than 400 Wh/kg.

Blackwing Sweden AB estimates that during the course of five years and 900 flight hours a professional flight school can generate up to 16% savings when investing in an electrical airplane instead of a combustion airplane.

The aircraft development process could be divided into an elementary outline as seen in figure 1.1, this project is conducted in the third step, preliminary design. The process is much more iterative and complex than is shown in figure 1.1, but gives an elementary overview.

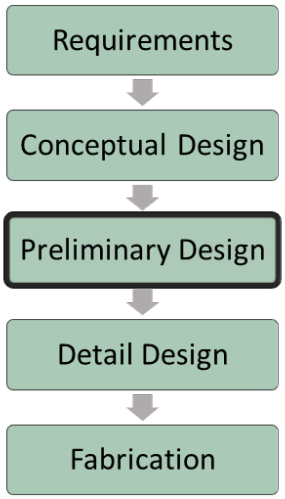

Figure 1.1: Flow chart displaying elementary aircraft development process, highlighting the step this project will work within.

1.2.1 Goals and Objectives

1. Model the aerodynamic performance of the existing wing and three potential wings.

The wing designed specially for an electric driven plane is called GreenWing (GW). The tools needed to create a new wing are expensive, thus Blackwing Sweden AB want to explore the option of using the existing tools to shorten and lengthen their current wing, Blackwing (BW).The altered wings will be referred to as BW Short (BW-S) and BW Long (BW-L). The different wings are seen in figure 1.2.

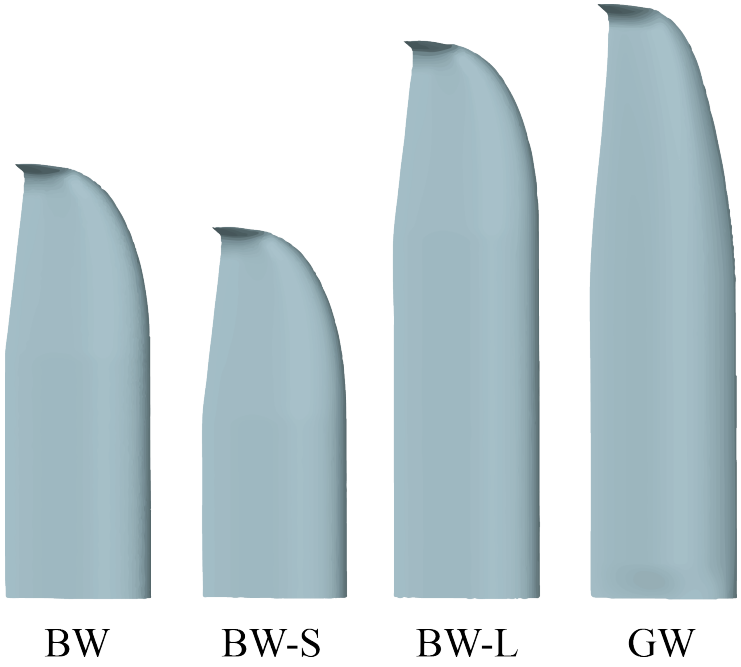

Figure 1.2: The four wings that will be modelled.

2. Provide a wing suggestion.

An evaluation of the four wings which compares stall progression and efficiency, as well as economical aspects of manufacturing the wings will be conducted. The results of the evaluation will be used to determine which wing has the highest potential.

3. Explore the achievement of the 2 h flight time target and competitiveness on the market.

The target set of 2 h flight time is to be evaluated, exploring what will be required in order to fulfill the requirement. How will adding extra batteries affect the airplane? What specific capacity of batteries is required?

Currently there are several prototypes of similar sized electrical aircrafts on the market, how does Blackwing Sweden AB's concept compare?

1.2.2 Delimitations

This project will not go into detail of the mathematics behind Computational Fluid Dynamics, CFD, or explore different turbulence models more than the selected Shear Stress Transport (SST) k-ω and Transitional SST models.

The properties that could be modeled using CFD are nearly endless, therefore the focus will lay on modelling the behaviours during cruise using a clean aircraft configuration.

The evaluation of the wings will not include other parameters such as the stability and maneuverability of the aircraft. These parameters are of importance, however the scope of this project is limited.

1.2.2.1 Modelling of the Propeller

The rotation of the propeller produces thrust, drag and torque. The drag component causes a propwash vortex sheet to emanate from each blade in a helical path that flows back over the fuselage, parts of the wing and the tailplane. The wings total lift is influenced by the total slipstream over the whole aircraft, plus the wing lift enclosed within the propwash. Therefore, the total amount of lift can be varied by varying the thrust of the propeller. Increasing the thrust will increase the propwash-flow over the wing thus increasing lift. Due to the additional lift from the propwash, the stalling speed can be lowered by 2.6-5.1 m/s compared to when power is off. [5]

However, since one important aspect for this project is the flow over the wing at high angles of attack (above 8°), when the backwash of the propeller is minimal, and since modelling the propeller using a virtual disk would add to the complicity of the model whilst doubling the number of elements needed, the propeller will not be modeled.

1.3 Outline of the Thesis

The first section "1. Introduction" contains the background needed to understand the problem presented, as well as the goals and objectives. The second section "2. Theoretical Framework" dives deeper into the underlying theory used in this study. Section "3. Method" describes in what manner the study was conducted, and motivates the manner chosen. Section "4. Numerical Setup" demonstrates the numerical setup for the aerodynamic simulations. The choice of models, mesh technique, domain, etc. are explained. The results are presented and discussed in section "5. Results and Discussion". The last section "6. Conclusion" presents the conclusions, discussing the achievement of the goals and objectives as well as aspects of future research.

2 Theoretical Framework

2.1 Flight in General

The forces that act on the airplane are seen in figure 2.1 where T, L, D and W are thrust, lift, drag and weight respectively. The lift generated is dependent on the shape of the wing, both on the length and on the airfoil [6]. In general a longer wing produces more lift, but also more drag.

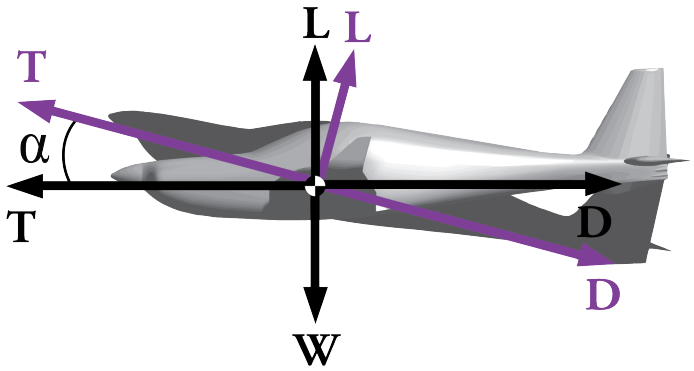

Figure 2.1: Lift, drag, weight and thrust effect on an airplane.

In cruise flight, the lift force equals the weight of the aircraft, thus maintaining altitude. Cruise flight implicates that an aircraft is traveling at a constant speed, i.e. the thrust force equals the drag force. Altering thrust allows for acceleration or deceleration, as well as climb or descent. The force components depend on the angle of attack, α, as seen in 2.1. The relationship between these forces is given in equations (2.1) and (2.2), where a_h and a_v are the horizontal and vertical accelerations and m is the mass of the aircraft. [7]

$$T \cdot sin(\alpha) - D \cdot sin(\alpha) + L \cdot cos(\alpha) - W = m \cdot a_v \tag{2.1}$$

$$T \cdot cos(\alpha) - D \cdot cos(\alpha) - L \cdot sin(\alpha) = m \cdot a_h \tag{2.2}$$

2.2 Airfoils

2.2.1 Flow Separation

When a flow separates from a surface, the pressure gradient is large enough to decelerate the flow close to the surface and eventually reverse it, as can be seen in figure 2.2. Thus a breakdown of the boundary layer occurs. On the surface of the wing, large, slow moving eddies are formed. What happens is that the pressure gradient switches from being favourable, where the pressure state aids the flow movement in the flow direction, to an adverse pressure gradient, where it instead retards the flow in the boundary layer. With an adverse pressure gradient the boundary layer therefore thickens, and eventually separates. [8]

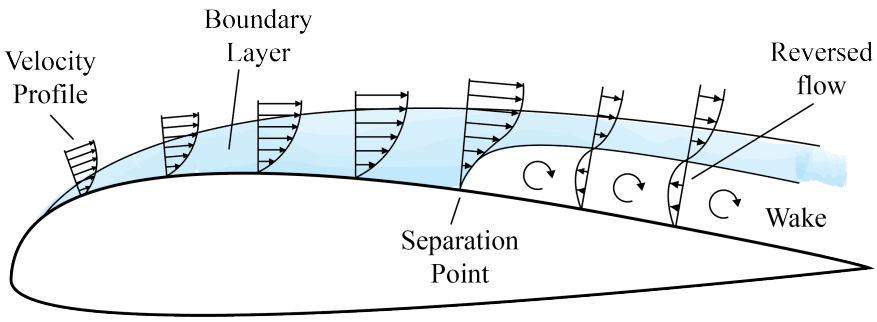

Figure 2.2: Flow separation progression over an airfoil, where the separation point is illustrated as well as the velocity profiles. Exaggerated to show phenomena.

The flow separation results in a large increase in minimum drag, and a large decrease in lift force. [9]

2.2.2 Laminar and Turbulent Airfoils

There are two main types of airfoils, laminar and conventional (turbulent). Laminar airfoils are taking advantage of the low viscous forces in the laminar boundary layer, leading to less drag (up to 50% reduction compare to fully turbulent airfoils [10]), however they are more prone to separation. Hence the choice of airfoil is a trade-off, largely dependent on the requirements of the aircraft. The two types of airfoils are seen in figure 2.3 where the transition point, X_{tr}, is marked. [11]

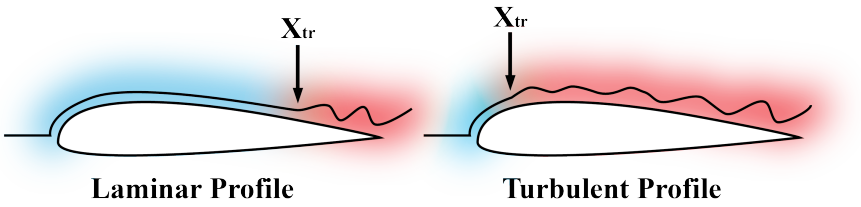

Figure 2.3: Difference in X_{tr} between laminar and turbulent airfoils.

Laminar airfoils are very sensitive and only work when the boundary layer can stay laminar, that means that any disruptions that alters the surface of the wing in form of dead bugs, water etc. will cause the flow to trip and become turbulent. Thus when manufacturing extra care is needed to make sure that any lap joints are completely filled and smooth and that the wings don't have any waviness or bumps. For the airplane to be safe, it must be able to fly in the case that the wing becomes contaminated during a mission. With a contaminated wing the drag is increased and the power needed from the aircraft to arrive to its destination is also increased. [10]

Turbulent airfoils have a higher drag, their advantage is that they are less prone to separation and thus more resilient to contamination on the wings. The requirements for constructing turbulent wings are less than those of laminar wings since the wing surface has less strict tolerances. [10]

2.3 Range and Endurance

Being able to predict range and endurance comes with discovering critical performance parameters, for instance, which velocity is suitable to travel the furthest.

When creating range and endurance estimations for an electrical aircraft, it is significant that the aircraft will not change its mass during the mission flight. The main outcome, in terms of modeling, is a simplified derivation for the range and endurance equations [1][2]. The range and endurance expressions derived here are specifically for an electrical airplane at the cruise stage of the flight mission, and do not take take-off, climb, descent and landing into consideration.

The range of an aircraft, R, in meters can be described by its flight speed, V_∞, and flight time, t, as seen in Equation (2.3).

$$R = V_\infty \cdot t \tag{2.3}$$

With the electric battery being drained during the course of flight, the flight time can

be connected to the time it takes to drain the battery. Under ideal conditions this can be expressed as in Equation (2.4).

$$t = \frac{m_{battery} \cdot E^* \cdot 60^2}{P_{battery}} \tag{2.4}$$

The total mass of the battery is dictated by $m_{battery}$, E^* is the mass specific energy, and $P_{battery}$ is the power drawn from the battery.

Inserting Equation (2.4) into Equation (2.3) yields Equation (2.5), that takes the battery drainage time into account.

$$R = V_\infty \cdot \frac{m_{battery} \cdot E^* \cdot 60^2}{P_{battery}} \tag{2.5}$$

Connecting the electric power available from the battery, $P_{battery}$, to the propulsive power, $P_{aircraft}$, and the systems efficiency (from battery to propulsive power), η_{total}, yields Equation (2.6).

$$P_{battery} = \frac{P_{aircraft}}{\eta_{total}} \tag{2.6}$$

The power required by the aircraft, is directly linked to the parameters of flight through the drag component, the velocity, and the coefficients of lift and drag, C_L and C_D, as seen in Equation (2.7)

$$P_{aircraft} = D \cdot V_\infty = \frac{W}{C_L/C_D} \cdot V_\infty \tag{2.7}$$

Combining Equations (2.5), (2.6) and (2.7), the resulting Equation (2.8) for range is achieved.

$$R = E^* \cdot 60^2 \cdot \eta_{total} \cdot \frac{C_L}{C_D} \cdot \frac{m_{battery}}{W} \tag{2.8}$$

Note the elimination of the flight velocity in Equation (2.8). This does not mean that the range is independent of the flight velocity, rather the velocity is affecting the equation indirectly through C_L and C_D.

The resulting Equation (2.8) for the range of an electrical aircraft reveals which of these parameters to maximize and which to minimize. In order to increase the range

the C_L/C_D ratio, the battery to total mass ratio, the mass specific energy and the systems efficiency are to be maximized.

The correlation between range and endurance, E, can be expressed as Equation (2.9).

$$R = V_\infty \cdot \frac{\eta_{total} \cdot E_{battery} \cdot 60^2}{P_{aircraft}} \Rightarrow E = \frac{\eta_{total} \cdot E_{battery} \cdot 60^2}{P_{aircraft}} \tag{2.9}$$

With this correlation the final expression for the endurance Equation (2.10) is derived. [1]

$$E = \frac{\eta_{total} \cdot E_{battery} \cdot 60^2}{W \cdot V_\infty} \cdot \frac{C_L}{C_D} \tag{2.10}$$

The derivation of Equations (2.8) and (2.10) are performed with assumptions that are necessary to mention. The voltage and the current are assumed to be relatively constant. The applicability in this estimation depends on if the current is below the maximum continuous current or not. This uncertainty is considered negligible. The final Equations (2.8) and (2.10) are only applicable for no-wind, steady, level cruise during which Equation (2.11) holds true. P_{REQ} is the power required to preserve level flight. [1]

$$P_{aircraft} = P_{REQ} = \frac{W}{\frac{C_L}{C_D}} \cdot V_\infty \tag{2.11}$$

The importance of the ratio between the lift and drag becomes apparent through the final Equations (2.8) and (2.10), thus emphasizing the need to further explore these parameters. It is also clear that the electrical motor, the propeller's efficiency and power output are essential in order to accurately predict range and endurance.

2.4 Drag

2.4.1 Drag sources

Drag is often described as a single quantity force, when in reality, the drag force on an aircraft has several sources. While some of these sources are difficult to model and predict, they are all of great importance for the creation of an accurate model. In order to describe these drag sources, the boundary layer needs to be defined.

2.4.1.1 Minimum Drag

Due to the friction between the air and the wing surface (as a consequence of viscosity), the fluid is brought to rest at the surface, a so called no slip condition. Within a small region from the surface the velocity rises rapidly from zero, to the free-stream velocity. This region is the boundary layer. The viscous stresses created within the boundary layer are of significance for the first two drag sources. [9]

If these viscous stresses are integrated tangentially over the wing surface, a force in the stream direction is given. This is the skin friction drag. In order to model skin friction drag it is important to predict the state of the boundary layer, and where flow separation occurs. This is mainly because the skin friction drag depends on the thickness of the boundary layer. [9]

If the pressure is multiplied by the normal direction, projected onto the flow direction and integrated across the surface of the wing, the pressure drag is given. The pressure distribution over an airfoil reveals that the pressure is lower at the trailing edge compared to the leading edge. That pressure difference gives a resulting force in the stream direction. [9]

In the case of a two dimensional airfoil, these two drag sources are the only drag contributors (except for wave drag that occurs at higher velocities). [9]

The skin friction drag and the pressure drag are together called the minimum drag, D_{min}.

2.4.1.2 Lift-Induced Drag

In the three dimensional case, with a finite wing, cross flow on the surface can be taken into consideration. When comparing the upper and lower surfaces of the wing, the pressure is generally lower on the upper surface and larger on the lower surface. By the wing tip, where the upper and lower surface meet, the pressure of the upper and lower surfaces tend towards each other, as can be seen in figure 2.4. This span wise pressure distribution causes a resulting velocity, a cross flow. The upper surface velocity moves towards the root of the wing, while for the lower surface it moves towards the wing tip. This results in a continuous vortex shedding along the trailing edge. This state of several smaller vortices is unstable, in practice they roll up to form a large vortex by the wing tip, as in figure 2.5. This vortex drains energy from the airflow, and is the source of what is called the lift-induced drag, D_i. [9]

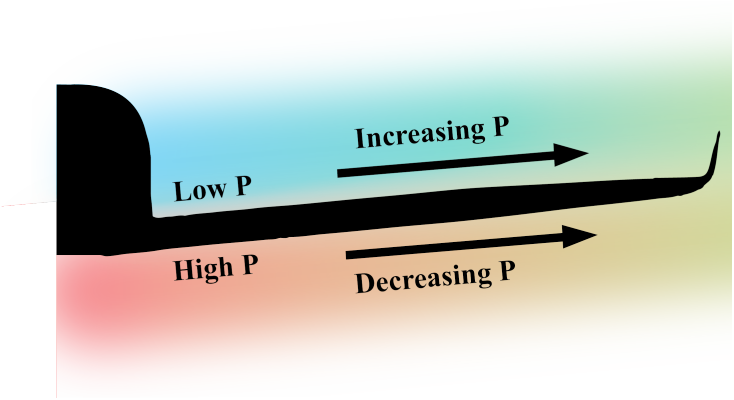

Figure 2.4: Span wise pressure distribution.

Figure 2.5: Wing tip vortex.

The drag force can now be expressed as the sum of these drag contributors as in Equation 2.12.

$$D = D_{min} + D_i \tag{2.12}$$

2.4.2 Drag Model

With the major drag forces introduced, a drag model can be described. There are different classes of drag models, and their usability solely depends on the flight case. What differs a simple and advanced drag model, is that the advanced model accounts

for boundary layer state, and regions that separate laminar to turbulent regions. An advanced drag model takes the point of flow separation into consideration, as well as the effects of deploying flight control and landing systems. Therefore a simpler model can not be used accurately if the flight case involves high angles of attack, or a transitional boundary layer. What remains an issue with the drag models however, independent of the class of the drag model, is the inaccuracy at high angles of attack. [1]

The coefficient of drag is a non-dimensional parameter related to D and S, the reference area of the wing, given an incompressible flow. The relation is given in (2.13).

$$C_D = \frac{2D}{\rho V_\infty^2 S} \tag{2.13}$$

Using C_D, the relation in Equation 2.12 can be rephrased as in Equation 2.14, which is the general expression of a drag model. $C_{D_{min}}$ is the minimum drag coefficent.

$$C_D = C_{D_{min}} + C_{D_i} \tag{2.14}$$

In a simple drag model C_{D_i}, the coefficient of induced drag, is defined as in Equation (2.15). [1]

$$C_{D_i} = k \cdot C_L^2 \tag{2.15}$$

k is the Lift-Induced drag constant, defined as Equation 2.16 in which e is the Oswald's span efficiency and AR is the aspect ratio.

$$k = \frac{1}{\pi \cdot AR \cdot e} \tag{2.16}$$

Whereas an adjusted drag model expresses C_{D_i} as in Equation 2.17.[1]

$$C_{D_i} = k \cdot (C_L - C_{L_{minD}})^2 \tag{2.17}$$

Where $C_{L_{minD}}$ is the lift coefficient at minimum drag.

2.4.3 Drag Polar

A drag polar can be created, see figure 2.6. The drag polar plots C_D as a function of C_L, given a set flight case with varying α. The drag polar allows identification of where a decrease in lift begins for a continuing increase in α and the D_{min} for a given

α. It also enables estimating the value for the highest $\frac{C_L}{C_D}$ ratio, which previously has been noted to be significant for range and endurance analysis.

It is noteworthy that the mentioned division of the coefficient of drag (minimum and induced drag), is not used in ANSYS Fluent. The software instead divides the drag contributors into viscous forces (skin friction drag), and pressure forces (pressure and induced drag). This is because the origin of the pressure forces for a three dimensional case are indistinguishable. Thus the minimum drag and induced drag can't be extracted directly from the software. A numerical method is therefore used to convert the drag forces into the desired groups, specifically for an adjusted drag model, since that is what will be used in the project.

The drag polar can be described as a quadratic equation as in Equation (2.18), where A, B and C are constants. [1]

$$C_D = A \cdot C_L^2 + B \cdot C_L + C \tag{2.18}$$

From Equation 2.18 a derivation can be made that results in Equation 2.19.

$$\left.\begin{array}{lcl} k & = & A \\ C_{L_{minD}} & = & -B/(2 \cdot A) \\ C_{D_{min}} & = & A \cdot C_{L_{minD}}^2 + B \cdot C_{L_{minD}} \\ & & +C \end{array}\right\} \Rightarrow C_D = C_{D_{min}} + k\,(C_L - C_{L_{minD}})^2 \tag{2.19}$$

The resulting expression in Equation (2.19) is a typical presentation of an adjusted drag model. [1]

Hence, the data points are converted and expressed as an adjusted drag model.

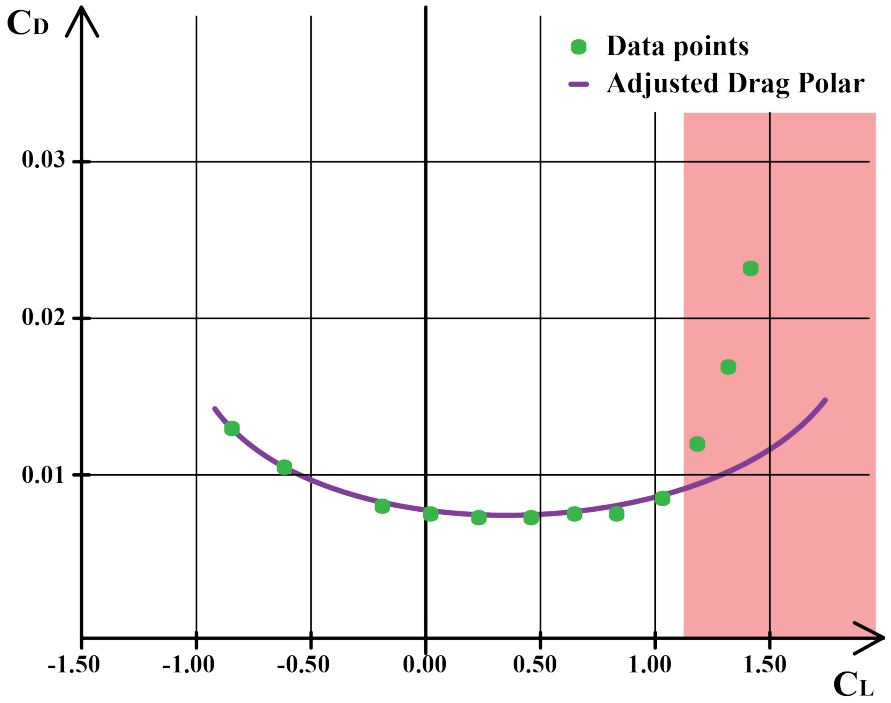

Figure 2.6: Drag polar including the curve for the adjusted drag polar, area of bad approximation marked in red. Example values.

2.4.4 Minimum and Induced Drag Forces Derived

In this section, expressions for D_{min} and D_i as functions of the velocity are derived. This is required to be able extract the total drag dependent on the velocity.

Given the expressions of $C_{D_{min}}$ and C_{D_i}, the drag components, D_{min} and D_i, can be derived as a function of velocity. Introducing the equivalent flat plate area f, allows $C_{D_{min}}$ to be expressed as in Equation (2.20). The equivalent flat plate area is a concept that helps calculate the drag of the aircraft. It assumes that the drag of the aircraft is equivalent to the drag of a plate moving normal to the flight path, with the same f and a $C_D = 1$. It is mainly used for comparing cases. [1]

$$C_{D_{min}} = \frac{f}{S} \tag{2.20}$$

Equation 2.20 disregards the effects of Reynolds and Mach number, which depending on the scenario may or may not be an appropriate simplification. [1]

$C_{D_{min}}$ can under certain circumstances be considered a constant, and the disregard-

ing mentioned above becomes acceptable. First of all, this is applicable if the aerodynamic body doesn't alter in shape or altitude and if there aren't compressibility effects present. [9]

Secondly, in the case of having a viscous flow, C_D (as well as C_L) have a dependency on the Reynolds number, Re. The dependency comes from the connection between Re, the boundary layer, and the lift and drag forces. The phenomena of laminar and turbulent boundary layers, and the transition between the two, is greatly affected by Re. More specifically, the location of the transition between the states is of interest when determining the dependency of the Reynolds number. Since both the drag and lift are dependant on the state of the boundary layer, even though the viscous contribution to the lift is minor, C_D and C_L's dependency on Re is given.[9]

If the Reynolds number effect on the boundary layer state could be considered negligible, within the Re range investigated, it would simplify the development of the drag polar, since the expression in Equation (2.20) would be considered acceptable. Since $C_{D_{min}}$ can be treated as a constant, f would in return also be a constant.

Furthermore, the equivalent flat plate area can be corrected, in regards to the cooling drag and miscellaneous drag. Equation (2.21) shows how the correction is made.

$$f_{CFD} + f_{Cooling} + f_{Miscellaneous} = f \tag{2.21}$$

This new f is then used to calculate the corrected $C_{D_{min}}$ (which in the future is just noted as $C_{D_{min}}$).

This correction is also used to account for skin friction drag, as well as interference between parts of the aircraft body [1]. Given the CFD setup, the two parameters do not need to be corrected.

Expressing f as a function of D_{min}, as below in Equation (2.22) where q_∞ is the dynamic pressure, equal to $\frac{\rho V^2}{2}$.

$$f = \frac{D_{min}}{q_\infty} \tag{2.22}$$

D_{min} can now be expressed as a function of the velocity, combining equations (2.20) and (2.22).

$$D_{min} = f \cdot q_\infty = \frac{C_{D_{min}} \cdot S \cdot \rho \cdot {V_\infty}^2}{2} \tag{2.23}$$

As for D_i, since the equations derived apply for a level flight in cruise, it means that the weight of the aircraft will be equal to the lift force, $W = L$.

If the derived expression from Equation (2.17) is used, it can now be expressed as in (2.24).

$$C_{D_i} = k \cdot (C_L - C_{L_{minD}})^2 = \frac{(C_L - C_{L_{minD}})^2}{\pi \cdot AR \cdot e} = \frac{\left(\frac{W}{q_\infty \cdot S} - C_{L_{minD}}\right)^2}{\pi \cdot AR \cdot e} \quad (2.24)$$

If expressed in D_i, this correlates to Equation (2.25).

$$D_i = q_\infty \cdot S \cdot \frac{\left(\frac{W}{q_\infty \cdot S} - C_{L_{minD}}\right)^2}{\pi \cdot AR \cdot e} = \frac{\rho \cdot V^2 \cdot S}{2} \cdot \frac{\left(\frac{2W}{\rho \cdot V^2 \cdot S} - C_{L_{minD}}\right)^2}{\pi \cdot AR \cdot e} \quad (2.25)$$

Adding equations (2.23) and (2.25) yields the total drag force as a function of the velocity, and can thus be compared to the available thrust force. The total drag force is given in Equation (2.26). [1]

$$D = \frac{\rho \cdot V^2 \cdot S}{2} \cdot \left(C_{D_{min}} + \frac{\left(\frac{2W}{\rho \cdot V^2 \cdot S} - C_{L_{minD}}\right)^2}{\pi \cdot AR \cdot e} \right) \quad (2.26)$$

Equation 2.26 reveals that D_i is dominant at lower velocities, while D_{min} is increasing with the velocity as in figure 2.7.

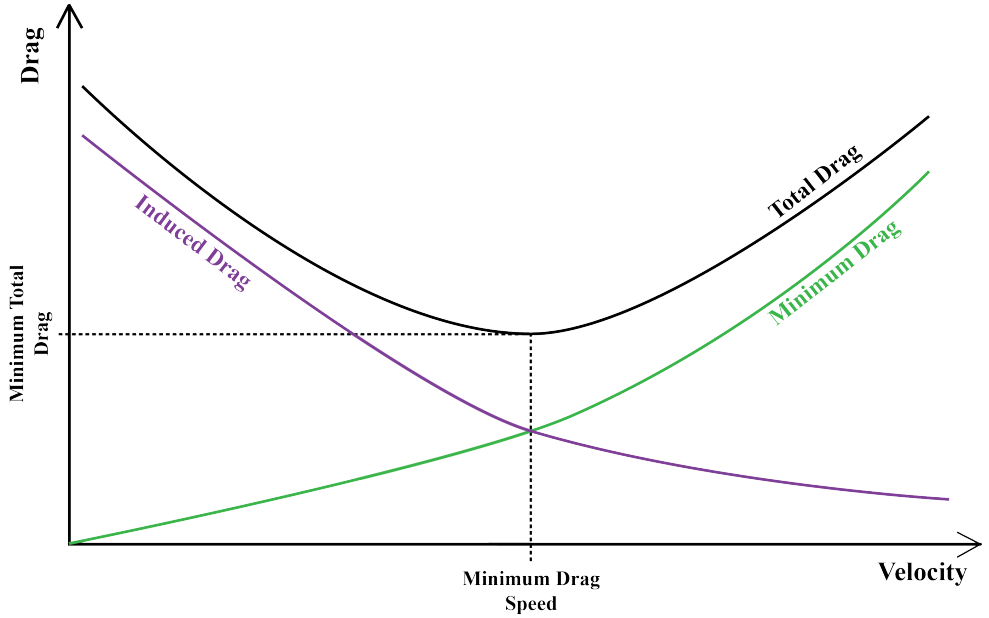

Figure 2.7: Minimum and Lift-induced Drag as a function of velocity.

2.4.5 Drag Prediction and Postdiction

The so far described procedures, are often part of a drag prediction analysis. It is usually conducted before the newly designed aircraft flies. With either flight data, or wind tunnel data, the model is then redefined and developed in a postdiction in order to match the measured data.

A usual refinement in the postdiction is to adjust the values of drag at higher angles of attack (as mentioned, the high absolute values of α often lead to inaccuracies). There are several methods to adjust the model due to the issue, where one of the more simple and reliable solutions is to introduce a quadratic spline into the drag polar once the model begins to highly underestimate the coefficient of drag. [1]

Another occurring refinement in the postdiction, which is relevant when developing the drag polar through CFD, is to account for the inaccuracies when modeling flow separation. It is not uncommon that the drag model needs to be adjusted by a constant value, i.e. for all angles of attack. [12]

2.5 Thrust

The propeller on the GW-plane is a constant-speed propeller, this type of propeller can change the angle of the propeller blades. Changing the angle of the blades allows the propeller efficiency to be high at both low and high speeds. The propeller efficiency, η_p, is calculated using Equation (2.27), where P_W is the engine power in W. [1]

$$\eta_p = \frac{T \cdot V_\infty}{P_W} \tag{2.27}$$

In the cases that η_p is known, Equation (2.27) can be used as a simple mean to calculate T, as seen in Equation 2.28. η_p is typically 0.85 in a constant speed configuration.[1]

$$T = \frac{\eta_p \cdot P_W}{V_\infty} \tag{2.28}$$

2.6 Thrust-Drag Relationship

Displaying the modelled thrust and drag together can be used to show the thrust-drag relationship as seen in the figure 2.8.

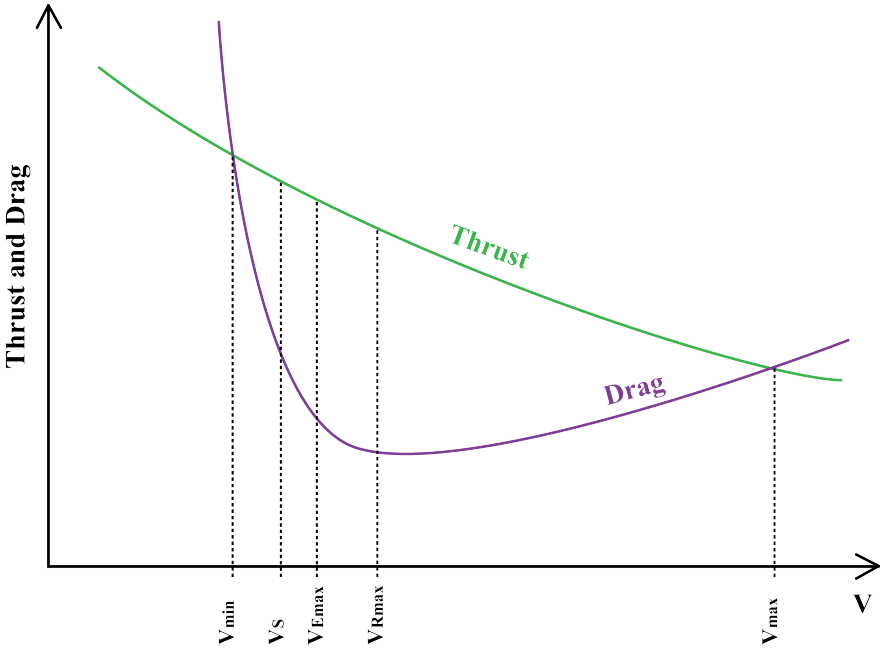

Figure 2.8: Thrust and drag curve including important velocities.

Combining the drag and thrust forces as a function of the velocity, visualizes the thrust available and, through the drag, thrust required to maintain level flight. Including data points for certain velocities, such as stalling speed V_S, best range speed $V_{R_{max}}$ and other important velocities help map the overall important airspeeds for cruise flight. For instance, the maximum and minimum airspeeds, V_{max} and V_{min}, are found where the two curves meet, since the thrust can't overcome the drag force. In between these extremes, the aircraft can accelerate and decelerate by adjusting the thrust effect.

Similarly, the power required can be displayed versus the power available, see figure 2.9. Again the maximum and minimum velocities are given, furthermore the velocity at which the power required is at its minimum is now identifiable.

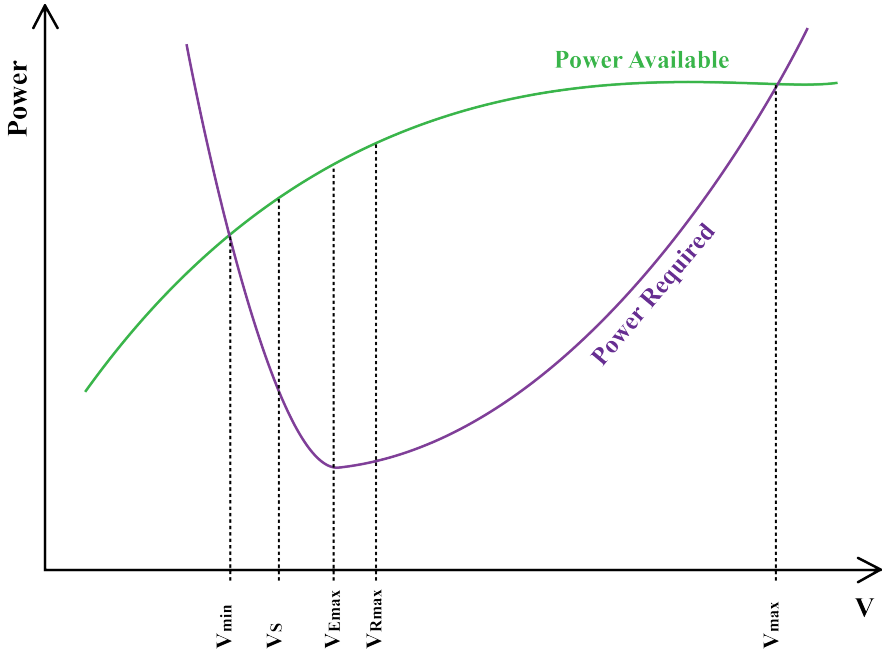

Figure 2.9: Power required and power available curve including important airspeeds.

2.6.1 Important airspeeds

2.6.1.1 Maximum and Minimum Airspeed

The thrust-drag curves display the available thrust, T_{AV}, as well as the required thrust to maintain the airspeed (the drag force), T_{REQ}. When the two curves meet, $T_{AV} = T_{REQ}$, it yields the two points where V_{max} and V_{min} are obtained.

Using Equation (2.28) as T_{AV} and Equation (2.26) as T_{REQ}, the relation can be described as in Equation (2.29).

$$T_{AV} - T_{REQ} = \frac{\eta_p \cdot P_W}{V_\infty} - \frac{\rho \cdot {V_\infty}^2 \cdot S}{2} \cdot \left(C_{D_{min}} + \frac{\left(\frac{2W}{\rho \cdot {V_\infty}^2 \cdot S} - C_{L_{minD}} \right)^2}{\pi \cdot AR \cdot e} \right) = 0 \tag{2.29}$$

A solution of Equation (2.29) can be obtained through an iterative scheme, solving for V_∞. Thus V_{max} and V_{min} can be found.

It is noteworthy, that V_{min} should be compared to V_S. In the case of V_S being higher than V_{min}, V_{min} is usually set equal to V_S. This is because, the stall velocity is the

minimum speed an aircraft can fly and maintain its altitude. [1]

2.6.1.2 *Airspeed of Maximum Lift-to-Drag Ratio, Airspeed of Minimum Thrust Required and Maximum Range Airspeed*

The airspeed of maximum lift-to-drag ratio, $V_{LD_{max}}$, also called the best glide speed, is of high importance in case of an engine failure.

The maximum lift-to-drag ratio, LD_{max}, can for an adjusted drag model be obtained through Equation (2.30). [1]

$$LD_{max} = \left(\frac{C_L}{C_D}\right)_{max} = \frac{1}{\sqrt{4kC_{D_{min}} + (2kC_{L_{min_D}})^2} - 2kC_{L_{min_D}}} \tag{2.30}$$

Moreover, the airspeed of maximum lift-to-drag ratio is given in Equation (2.31). [1]

$$V_{LD_{max}} = \sqrt{\frac{2}{\rho}\left(\frac{W}{S}\right)\sqrt{\frac{k}{C_{D_{min}} + kC_{L_{min_D}}^2}}} \tag{2.31}$$

This airspeed is also called the airspeed of minimum thrust required, $V_{TR_{min}}$, since the velocity is found at the minimum drag force (hence minimum thrust required). This specific airspeed also divides the regions of speed stability and instability, where a lower velocity is in the unstable speed region and a higher velocity is in the stable speed region.

For a propeller driven aircraft, it can be shown that $V_{R_{max}}$ occurs at LD_{max}. Meaning that $V_{LD_{max}}$ equals $V_{TR_{min}}$ and $V_{R_{max}}$. [1]

2.6.1.3 *Airspeed of Minimum Power Required and Maximum Endurance Airspeed*

The power required, P_{REQ} has since earlier been defined as in Equation (2.11). The velocity where the P_{REQ} is at its minimum, is called $V_{PR_{min}}$.

It can be identified by using figure 2.9 at the minimum required power.

In the case of a propeller driven aircraft, this airspeed is equal to the airspeed at which maximum endurance, $V_{E_{max}}$, can be achieved. Thus the final relation is presented in Equation (2.32). [1]

$$V_{PR_{min}} = V_{E_{max}} \tag{2.32}$$

With $V_{E_{max}}$ known, Equation (2.33) identifies the Lift-to-Drag ratio at the given velocity, given a steady flight.

$$LD_{Emax} = \frac{W}{D_{V_{E_{max}}}} \tag{2.33}$$

Note that Equation (2.33) is derived from Equation (2.11).

2.7 Wing stall

The flow separation at higher angles of attack is inevitable, it cannot be removed with a well designed wing. However, there are some aspects which are important in order to stall the aircraft in a certain way.

First of all, the stall should progress slowly. When the stall progresses and the lift starts reducing, it provides a feedback to the pilot. In case this progression is too rapid, it will be harder for the pilot to react to the changes. Secondly, it is important where the stall progresses on the wing. A desired appearance of the stall progression is that it begins in the root of the wing, and then spread out on the wing. This is desirable, since the lift reduction that occurs will be near the rolling axis of the aircraft (if one wing stalls before the other for instance). Thus the rolling tendencies are greatly reduced. In case the flow is separated near the ailerons, which are positioned further out on the wing, this results in a lateral control loss. Furthermore, in the case of a wing that stalls near the wing-tips, this can result in a pitch-up, where the angle of attack is increased as a result of the lift loss. From a safety point of view the wing should therefore begin stalling near the root of the wing, to avoid the dangerous characteristics that come with a separated flow by the wing tips. [9]

2.8 Electrical Aircraft Market

When jet engine fuel is used, it releases CO2 emissions, as well as non-CO2 emissions that also contribute to climate change. The air quality near ground is highly affected, increasing the total premature mortalities per year. The noise generated from an aircraft has also proven to result in adverse health impacts. [13]

A study was conducted where, assuming a battery mass specific energy of 800 Wh/kg, CO2 emissions for an electrical aircraft were calculated to be up to 30 percent lower compared to a typical similar sized jet aircraft. The study expected noise levels to be reduced overall as well. Moreover, the emissions would not be generated while in flight, but instead created when generating the electricity, thus allowing better control of the emissions. The author of the study estimates the 800 Wh/kg tar-

get to be reached around mid-century. This study was conducted when the highest $E_{battery}$ available was 250 Wh/kg. [13]

All in all, the study showed the potential of going electric in aviation (especially short flight missions), however emphasizing on that the battery mass specific energy today isn't yet competitive compared to the jet engine. Another study managed to, in lab conditions, create a battery reaching 500 Wh/kg [14].

2.8.1 Benchmarking

On the market there are some similar single front propeller competitors, for example Bristell Energic by Bristell and eFlyer 2 by Bye Aerospace. Both the planes are in the development stage with existing flying prototypes.

Data from these aircraft are extracted and summarized in table 2.1.[15][16][17][18]

Table 2.1: Benchmarking

	Bristell Energic	*eFlyer 2*
Stall Speed	24 m/s	24 m/s
Max Speed	56 m/s	69 m/s
Endurance	1.5 h	3 h
Range	-	400 km
Engine Power	80 kW	100 kW
Max take-off weight	850 kg	826 kg

3 Method

Through CFD the four wings aerodynamic behaviour will be modeled. As mentioned earlier, a postdiction is often created, taking wind tunnel data or flight data into consideration in order to refine and confirm the model. For the previous, combustion driven aircraft model BW there exists flight data. By performing the same CFD analysis with BW, the CFD results can directly be compared to flight data and to GW. Hence, the CFD model can be corrected using the previous aircraft and its flight data. Note that all four aircraft have the same fuselage exterior design, having only the wing altered between the four designs.

The model will first be created using a two equation based SST k-ω turbulence model commonly used to model airplanes, and then the more complicated four equation based Transitional SST turbulence model. The SST k-ω model is faster and therefore it is easier to find the base settings. The more complicated model is required to accurately be able to model the transition from a laminar boundary layer to a turbulent boundary layer that occurs on these laminar airfoils. The model will first be in 2D, once the models work for both turbulence models, the results will be compared to Xfoil and 3D models will be created.

Since the Transitional SST model is time consuming (given that it requires a finer modelling of the boundary layer), a correction factor will be used from the BW Transitional SST results, to estimate the BW-L and BW-S results. The similarities between the three BW wings was found to justify the correction method, without impairing the accuracy of the results. The process of estimating BW-L and BW-S is presented in detail in 5. Results and Discussion.

The data extracted from the models will be used to analyze the performance of the wings based on the how the separation propagates, the lift and drag as well as the range. Blackwing Sweden AB have a goal of 2 h flight time, how well these wings fulfill that goal will be examined and one wing will be selected.

The whole process is summarized in figure 3.1.

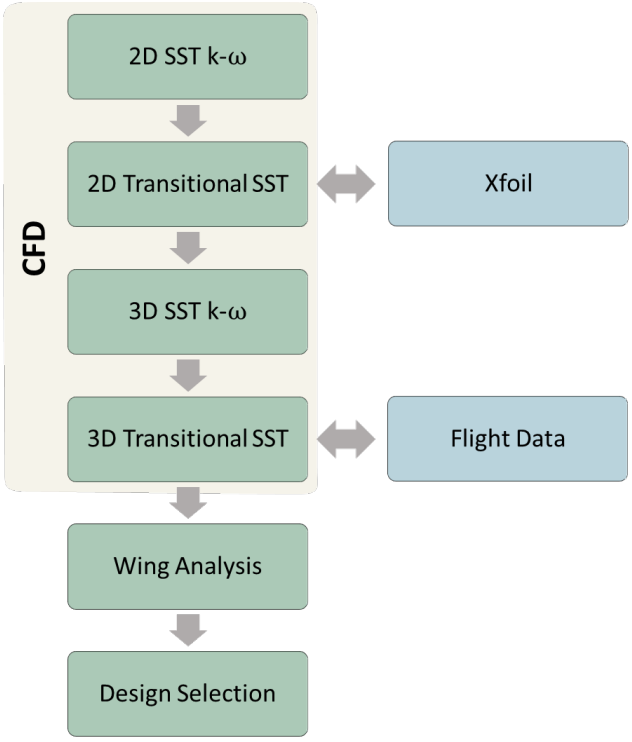

Figure 3.1: Flow chart displaying method.

4 Numerical Setup

The numerical analysis has been conducted using Ansys Fluent 2020 R1 and Ansys Fluent 2021 R2 for the CFD analysis.

4.1 CFD Analysis

4.1.1 Domain and Boundary Conditions

The domain is conic shaped, according to the recommendations for external aerodynamics and aerospace analysis [19]. The basic domain is seen in figure 4.1. The shape of the domain allows the attack angle to be varied (up to 20°) be varying the components of the velocity, this method was chosen as it doesn't require the remeshing of the model for every attack angle, as angling the airplane would.

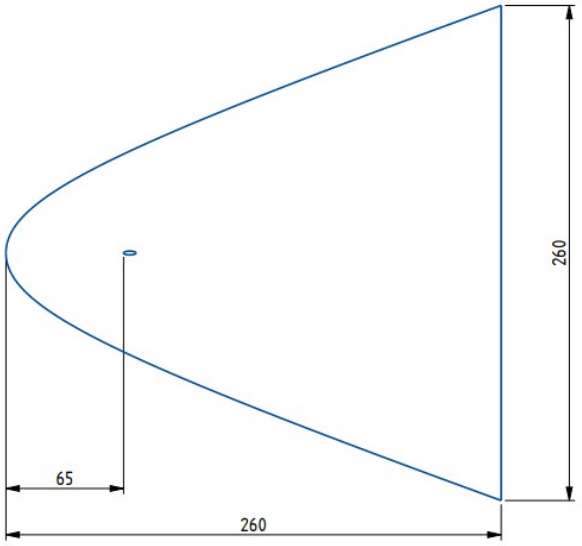

Figure 4.1: Overview of domain measured in meters.

The conic arc is set to a velocity inlet and the downstream boundary is set to a pressure outlet with a gauge pressure of zero. A half-body with a symmetry plane was used to model the symmetric flow. [19]

4.1.2 Turbulence Model

For the simulation setup, a Reynolds Averaged Navier Stokes, RANS, turbulence model is found to be sufficient. The large domain, combined with the near wall modelling makes the initial setup computationally expensive. The RANS models can obtain the average of all resolved flow features, which is sufficient when not having time dependency (i.e. no moving parts or periodic behaviour in the flow), and has a relatively low computational cost [20]. In cases of higher angles of attack, periodical behaviour in the form of separating and reattaching flow on the wing is possible. In these cases, steady state is no longer applicable, instead a time transient solution is necessary.

When it comes to aerospace RANS choices, the SST k-ω turbulence model is popular [21]. It performs well when investigating boundary layers with strong pressure

gradients, while still being able to handle free-stream flows [22].

One limitation of the standard two equation SST k-ω is that it assumes that the boundary layer is fully turbulent. The actual boundary layer state for the wing profiles is firstly laminar and then shifts to turbulent. In figure 4.2, the percentage of the boundary layer that are laminar for the wing profiles of GW and BW are presented. The two profiles have a clear difference in percentages of laminar boundary layer, especially on the suction side, thus being of importance to fully compare the wings without an error in the resulting forces from the skin friction. The four equation Transition SST is a model that adds equations in order to resolve where the boundary layer transitions to being turbulent [23].

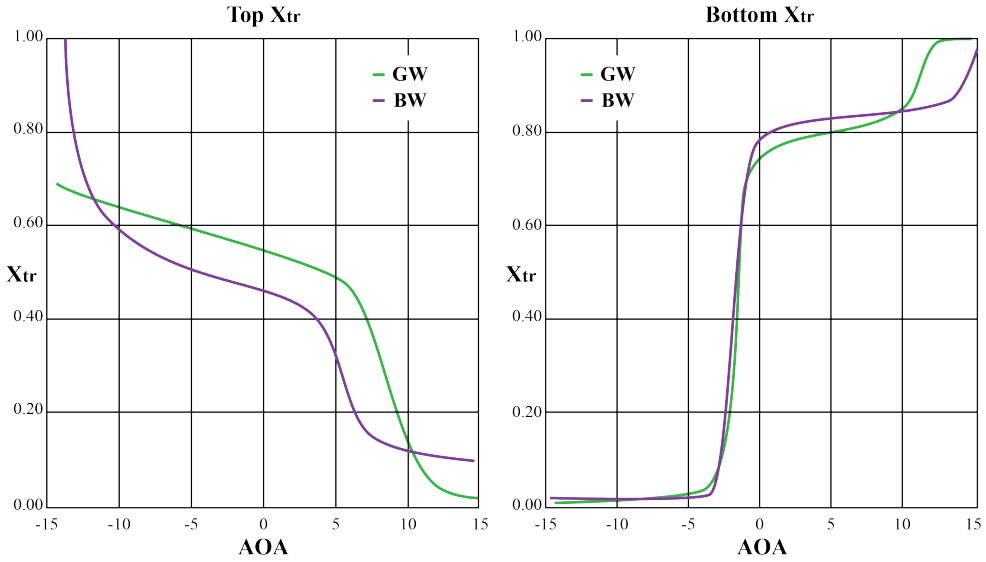

Figure 4.2: Transition point, X_{tr}, of boundary layer from laminar to turbulent. Top- and underside of the GW and BW wing profiles, normalized value.

4.1.3 SST k-ω Setup

4.1.3.1 Mesh Setup

The initial mesh setup is based on the desired y+ range and to capture the developed flow. In order to achieve a full resolution of the boundary layer, it is recommended to have the first grid point at $y+ \approx 1$ and required to be $y+ < 5$ [24]. The $y+$ is a measurement of how well the boundary layer is resolved, with a lower $y+$ the boundary layer is more resolved. The boundary layer cells are evaluated through looking at the velocity gradients starting from the surface of the wing, confirming that the fast increase of velocity is captured in the inflation as seen in figure 4.3.

The boundary layer cells are dependent on the mesh sizing set on the surface. An inadequate (i.e. too coarse) sizing on the surface mesh surrounding the boundary layer, results in skewed boundary layer cells. Skewness quality can be problematic, and the probability of a diverging result increases [23]. Due to this, an iterative meshing procedure was conducted, where the boundary layer settings as well as the mesh sizing of the aircraft were altered. The y+ range and the velocity gradients on the suction side on the wing are presented in figure 4.3 and figure 4.4.

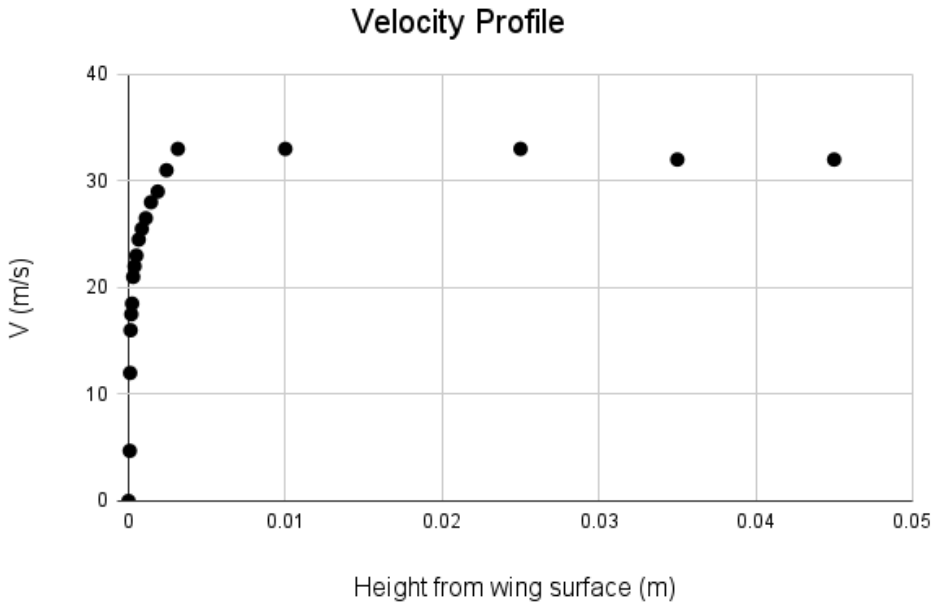

Figure 4.3: Plot of velocity dependent on distance from wing surface.

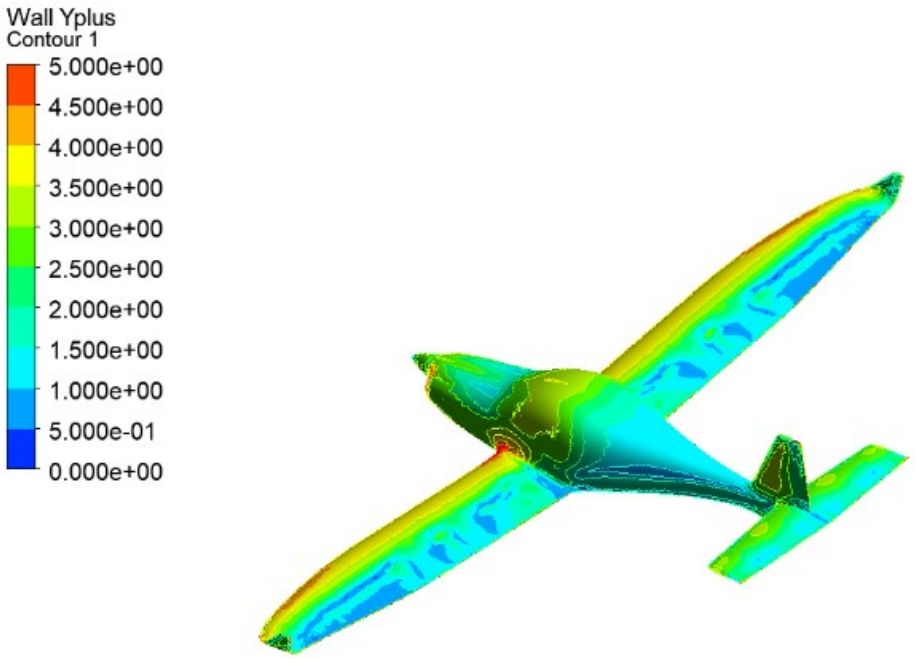

Figure 4.4: y+ value at α = 11°.

The wake created behind the airplane requires finer elements to model the flow. Hence seven body of influence's, BOI's, are included in the model to refine the mesh in the anticipated wake, seen in figure 4.5. The four BOI's closest to the aircraft are finer than the three behind them. Cross sections of the flow were studied to ensure that the BOI's covered the anticipated wake.

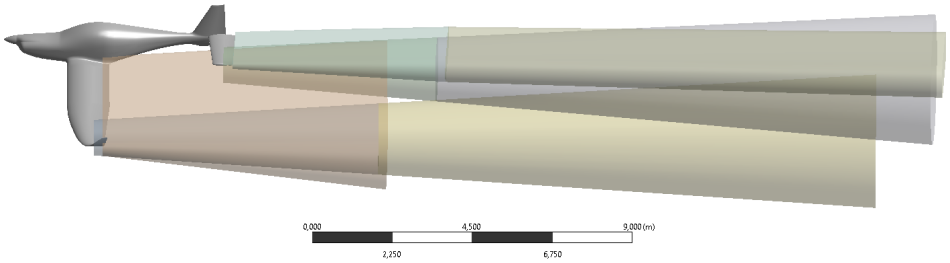

Figure 4.5: Body of Influence's.

4.1.3.2 *Mesh Sensitivity Analysis*

To ensure adequate mesh sizing in terms of numerical accuracy and computational cost, a mesh sensitivity analysis was performed.

For this analysis the sizing of the BOI's are varied to determine the influence of the mesh quality. The two most important parameters C_D and C_L for the coming analysis of the separation and drag induced are studied. Figure 4.6 show the variation depending on the amount of cells. Note that the y-axes in both 4.6a and 4.6b represent a change of five percent from the lowest value. The difference in C_D from the first point with 9 million cells to the second point with 18 million cells is 2.85%. Between the second point and the third point with 77 Million cells is less than 0.35% for both C_D and C_L, thus the second point is deemed the most appropriate in regards to accuracy and computational time.

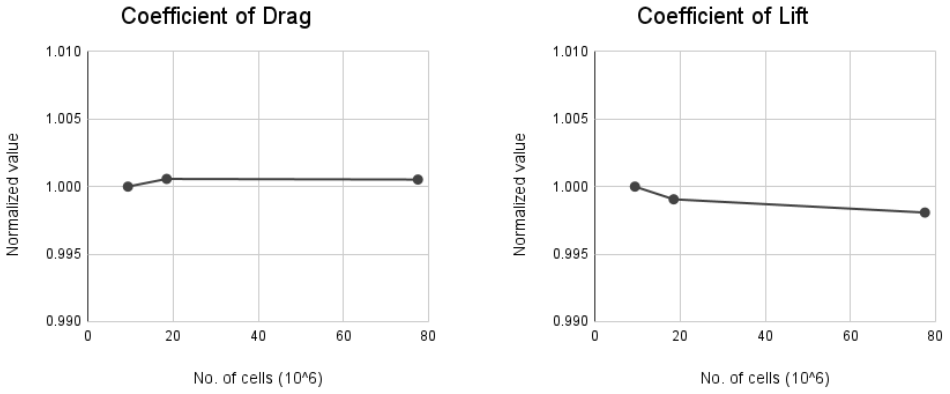

(a) C_D **versus no. of cells** **(b)** C_L **versus no. of cells**

Figure 4.6: Mesh Analysis C_D **and** C_L **normalized to first value.**

4.1.4 Transitional SST Setup

A 2D model using the Transitional SST turbulence model of GW was created before moving on to 3D. This was done to determine the accuracy of the model compared to the results from the program Xfoil, as well as to understand the behaviour that can be expected from the 3D model.

4.1.4.1 *Mesh Setup*

Unlike the SST k-ω turbulence model where $y+ < 5$, the Transitional SST turbulence model requires $y+ < 1$ in order to accurately predict the transition [23]. This requires the mesh to be refined, however refining the polyhedral mesh used for the

SST k-ω model was deemed problematic due to computational limitations.

A general problem when it comes to volume meshing with a fully resolved boundary layer, is the transition between the mesh cells. Different types of cells (hexahedral, polyhedral, tetraherdral, etc.) all come with their own advantages, and the optimal solution often is a combination of different elements. In practice, it can be difficult to create these hybrid meshes manually without the large increase in computational power required. A hybrid model that combines different element types was therefore chosen. The Poly-hexcore was originally created to reduce computing time and simplifying the meshing process by filling the bulk region with hexahedrals, maintaining the boundary layer poly prism modelling, while connecting the two areas with polyhedral elements. Studies have shown a significant decrease in cell count and computing time with the hybrid meshing model. Simultaneously, this allows for element transitioning to be made automatically. [25]

The final mesh was only refined on the wing, while retaining the settings on the body of the aircraft. This was deemed acceptable since the most important transition occurs on the wing. The velocity dependent on height from surface plot is seen in figure 4.7 and the y+ value is seen in figure 4.8.

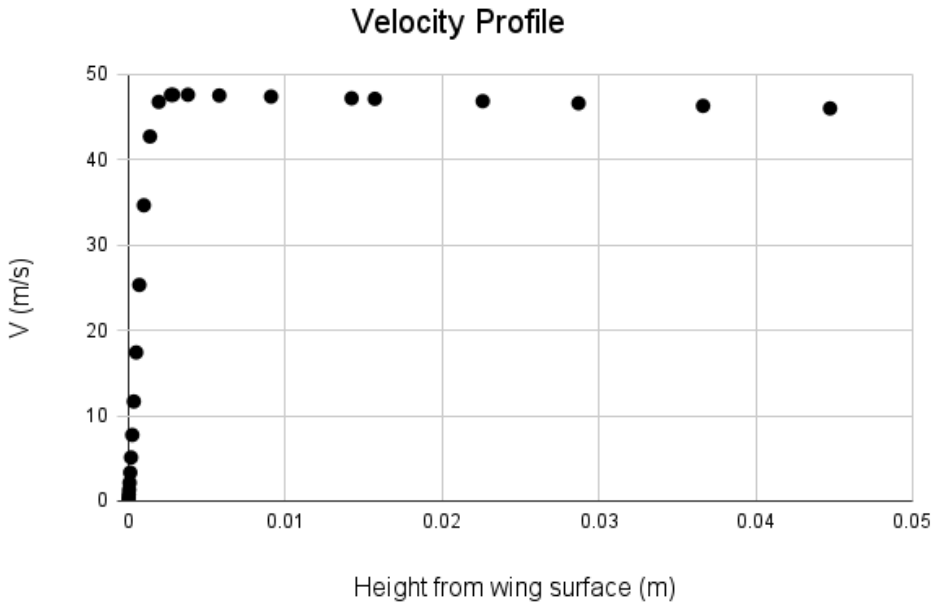

Figure 4.7: Plot of velocity dependent on distance from wing surface.

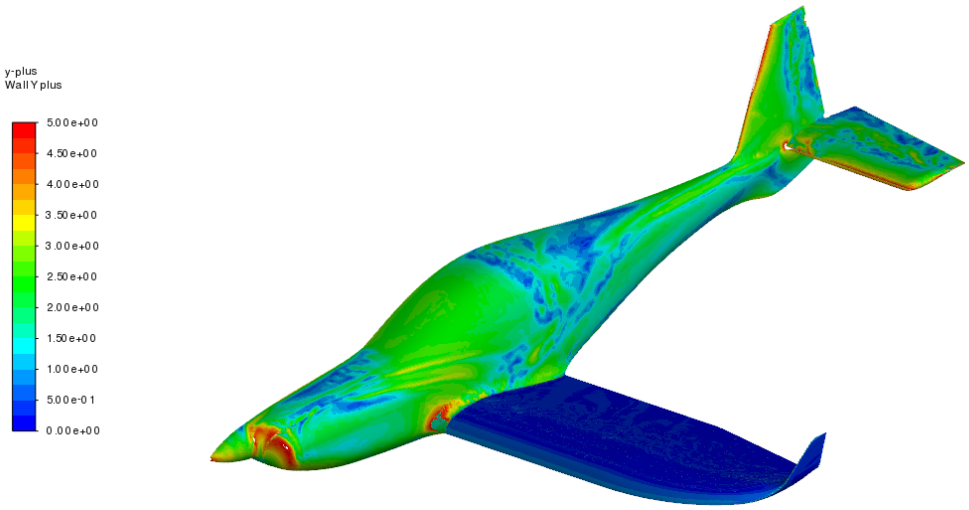

Figure 4.8: y+ value for BW at $\alpha = 11°$.

The final mesh is seen in figure 4.9.

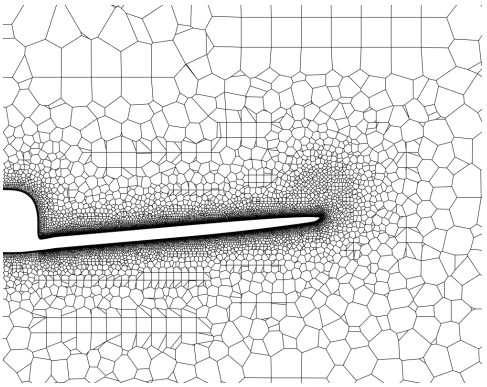

(a) Cross section of mesh.

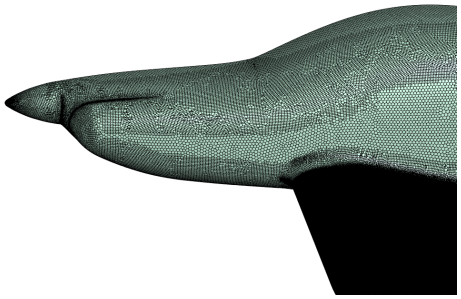

(b) Surface mesh on wing and aircraft body.

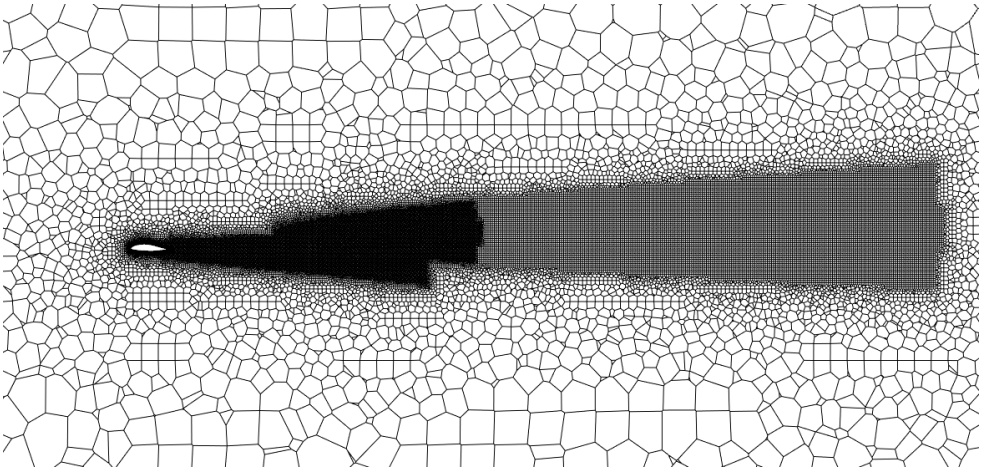

(c) Cross section of mesh displaying the wing and the BOI's influence.

Figure 4.9: Mesh.

5 Results and Discussion

5.1 Validation of Model

5.1.1 Adjusted Drag Model

A 2D study was conducted with varying velocities at cruising angle of attack in order to evaluate if the simplification of the drag model can be made with negligible errors. The transition point was compared in the range of approximated V_{min} and V_{max}. The study is presented in figure 5.1. The difference of X_{tr} between V_{min} to V_{max} is negligible, totaling to only 2.8%. Thus it is concluded that the study showed a low Reynolds number effect on the transition point, and equation (2.20) dictating that a constant $C_{D_{min}}$ is deemed acceptable.

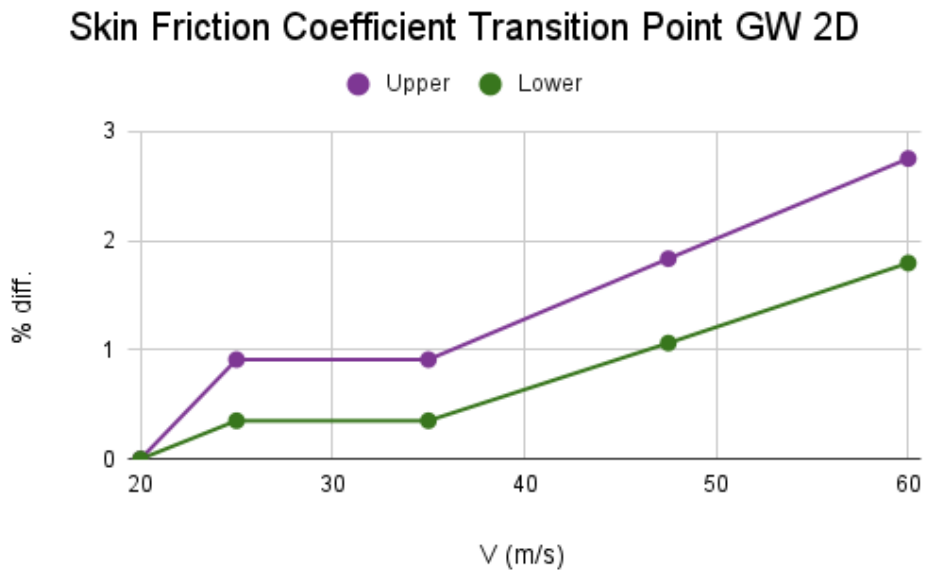

Figure 5.1: Skin friction coefficient at the transition point with varying velocities seen as percent difference from value at 20 m/s.

5.1.2 Validation Using 2D Simulations

Before the Transition SST model was used for the 3D case, the model was tested in a 2D simulation on a cross section of GW. This would allow a quick comparison between the SST k-ω model and the Transition SST model in 2D, but it would also allow comparison of the transition between laminar and turbulent boundary layer between 2D and 3D. Furthermore, the 2D simulation can indicate at which angle of attack, AOA, the flow is prone to separate.

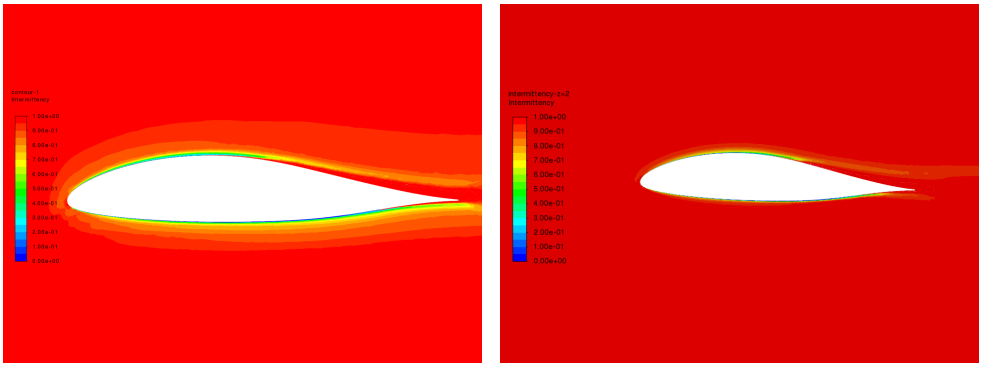

(a) Intermittency AOA=8° 2D **(b) Intermittency wing AOA=8° 3D**

Figure 5.2: Intermittency contour comparing the Transitional SST model for 2D and 3D.

Comparing the flow of the 2D model to a cross section of the 3D model it was noted that the transitions point was roughly the same however it occured later in the 3D model. One comparison is seen in figure 5.2. The intermittency ranges from 0 to 1 and is defined as the fraction of time the flow is turbulent. A value of zero dictates that the flow in that point is rarely turbulent and a value of one means that it is mostly turbulent. Thus where the value switches from 0 to 1 could be considered the point where the flow switches from laminar to turbulent. The difference between the two models could be derived from that the 2D case doesn't take cross flow into consideration. The conclusion is that the boundary transition in the 3D case was found sufficient, but should be investigated.

5.1.3 Model Accuracy

5.1.3.1 Time Transient Solution

In the iterative procedure of creating the model for the four wings, it was found that at higher AOA vortex shedding started to occur. A steady state solution could thus not be used since the results are time dependent and could therefore not converge.

Therefore it was deemed that a time transient solution was necessary to accurately model the case at higher AOAs. The time transient solution requires a lot of extra computer resources, compared to a steady state solution. That being the case, a time transient solution was not attempted. The cases with a higher AOA where flow separation is present, in the presented results this refers to BW AOA 11°, the results didn't converge and therefore have to be looked at with caution.

5.1.3.2 Mesh Sensitivity Analysis

The mesh sensitivity analysis that was conducted for the SST k-ω model was performed at an AOA of two degrees. The reasoning behind this was that the lower AOA cases converged well, and faster, resulting in saved computing time. However it was later understood that the analysis should have been done at a higher angle of attack, since the high AOA results have more tendency to alter depending on the mesh size. A mesh study done at the highest AOA would indicate a mesh independence at all AOAs. The mesh study was only conducted by varying the size of the BOI's to ensure that the vortices created behind the aircraft were resolved. Studying the resolution of the vortices at higher AOA the vortices were deemed resolved and thus the results from the mesh study were regarded applicable.

5.2 SST k-ω Compared to Transitional SST

The difference between the two turbulence models can be seen in figure 5.3. The difference between the two turbulence models is larger for GW since the profile is more laminar compare to BW's profile, as seen in figure 4.2. Since the Transitional SST model doesn't assume a fully turbulent boundary layer, as the SST k-ω model does, the difference between the models for the BW and GW wings are reasonable and expected. The earlier the transition from laminar to turbulent occurs the more alike the models are.

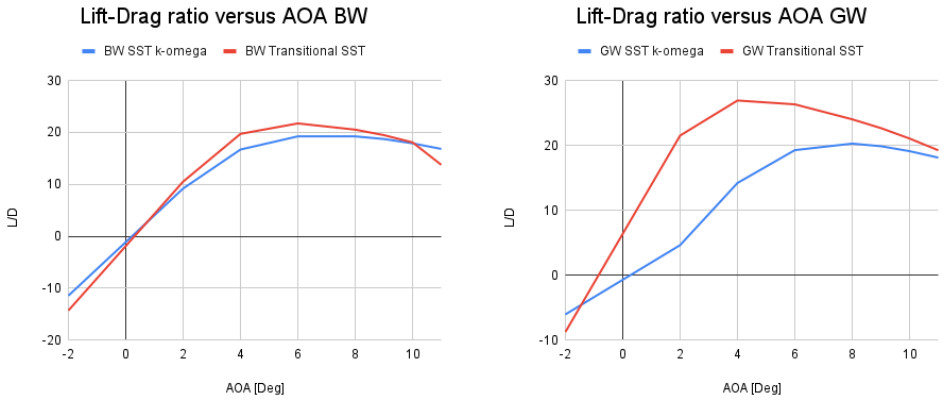

(a) L/D ration vs AOA for BW comparing SST k-ω to Transitional SST.

(b) L/D ration vs AOA for GW comparing SST k-ω to Transitional SST.

Figure 5.3: L/D ratio vs AOA comparing SST k-ω to Transitional SST.

The correction of BW-L and BW-S was made using a correction factor at each AOA, based on the Transitional SST model and the SST k-ω model results for BW. For example, the conversion at a given AOA to get $C_{D_{BW-L,Transition}}$ is given in equation (5.1).

$$C_{D_{BW-L,Transition}} = \frac{C_{D_{BW,Transition}}}{C_{D_{BW,SST}}} \cdot C_{D_{BW-L,SST}} \tag{5.1}$$

5.3 Flow Progression

5.3.1 Transition Point

By creating contours of the wall shear stress in the flow direction the transition point can be seen across the wing as a line. The wall shear stress contours for the low pressure side of BW are seen in figure 5.4. The transition point is seen moving forward with increasing AOA. Comparing the results to figure 4.2 the transition point occurs later in the 3D case than the 2D case. As mentioned previously, for BW AOA 11° the solution did not reach convergence, as can be seen in figure 5.4d the flow is reversed in several places across the wing. The transition point on the pressure side, figure 5.5, of the wing is fairly constant, much like figure 4.2.

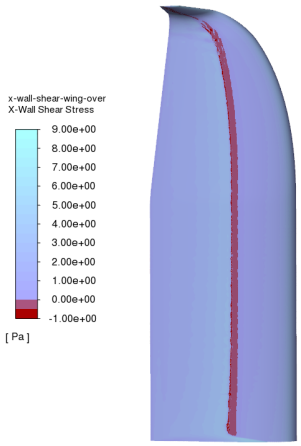

(a) BW AOA=2

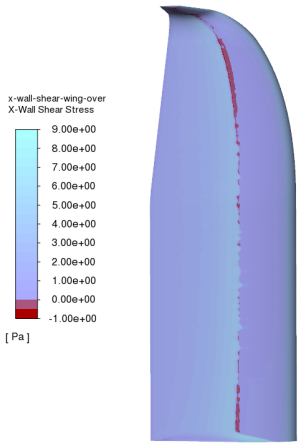

(b) BW AOA=8

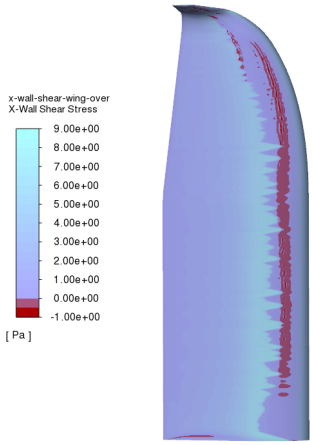

(c) BW AOA=10

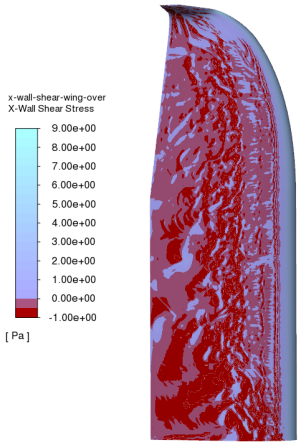

(d) BW AOA=11

Figure 5.4: Wall shear stress in flow direction for BW on the low pressure side of the wing.

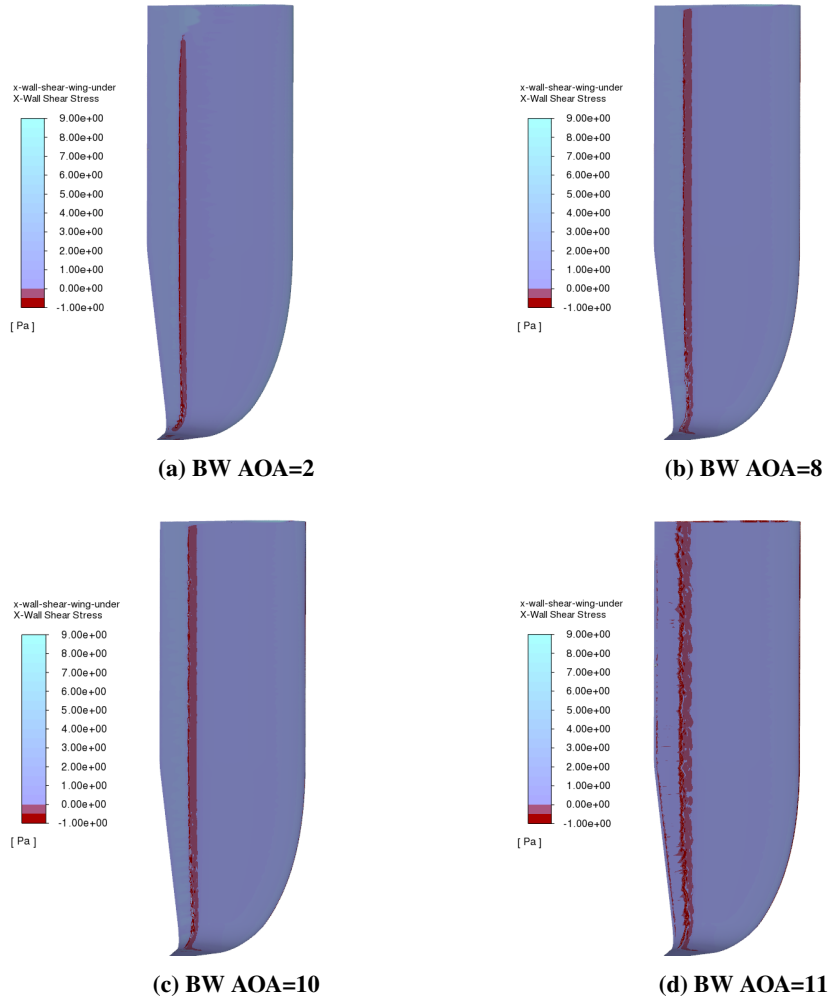

(a) BW AOA=2 **(b) BW AOA=8**

(c) BW AOA=10 **(d) BW AOA=11**

Figure 5.5: Wall shear stress in flow direction for BW on the high pressure side of the wing.

The same comparison could be done for the GW wing using figure 4.2 and figures 5.6 and 5.7. The high pressure side behaves similar to that expected from figure 4.2, the transition point is moved backwards with increasing AOA. Increasing the AOA to 9° would move the transition point quickly forward based on figure 4.2, however is not the results in the 3D case. The low pressure side of the wing corresponds to figure 4.2 well for the lower AOA, however for the higher AOA the transition occurs earlier than expected. When looking at figure 4.2 and comparing it to the 3D case, the behaviour is the same for both GW and BW with a 4° difference. An AOA of 2° corresponds to the behaviour of an AOA of -2° in figure 4.2. Notable is also the

back flow that is starting to spread from the root of the wing increasing from figure 5.6c to figure 5.6d.

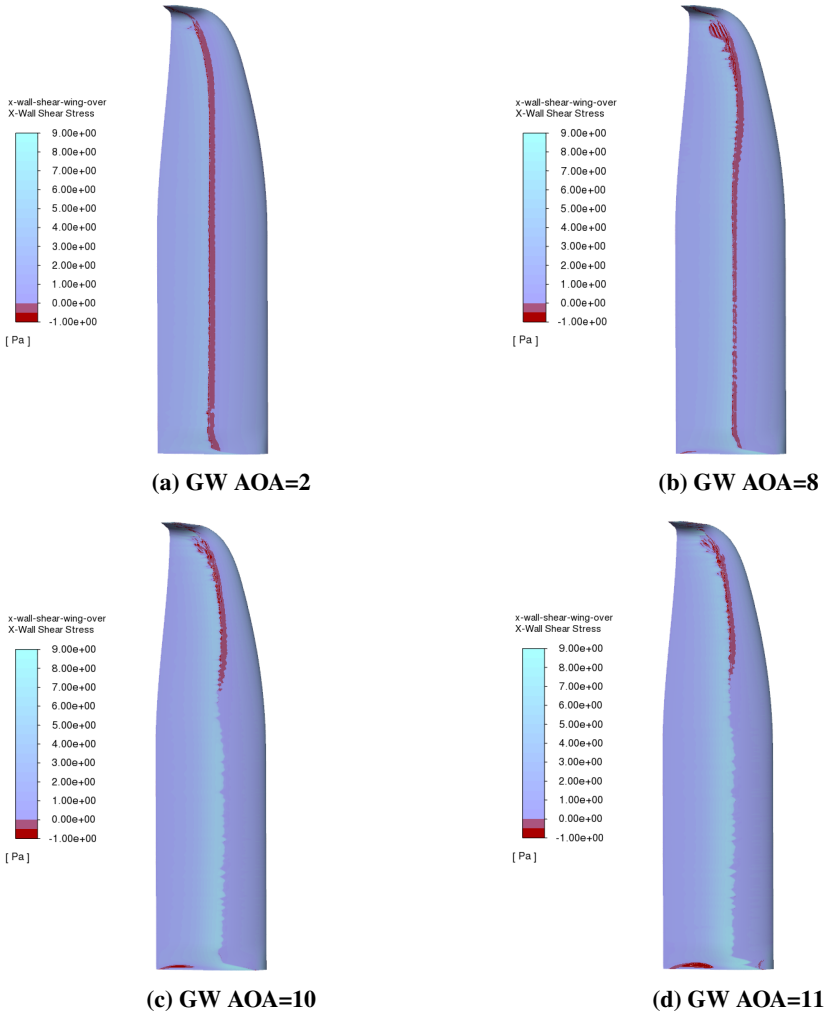

(a) GW AOA=2 **(b) GW AOA=8**

(c) GW AOA=10 **(d) GW AOA=11**

Figure 5.6: Wall shear stress in flow direction for GW on the low pressure side of the wing.

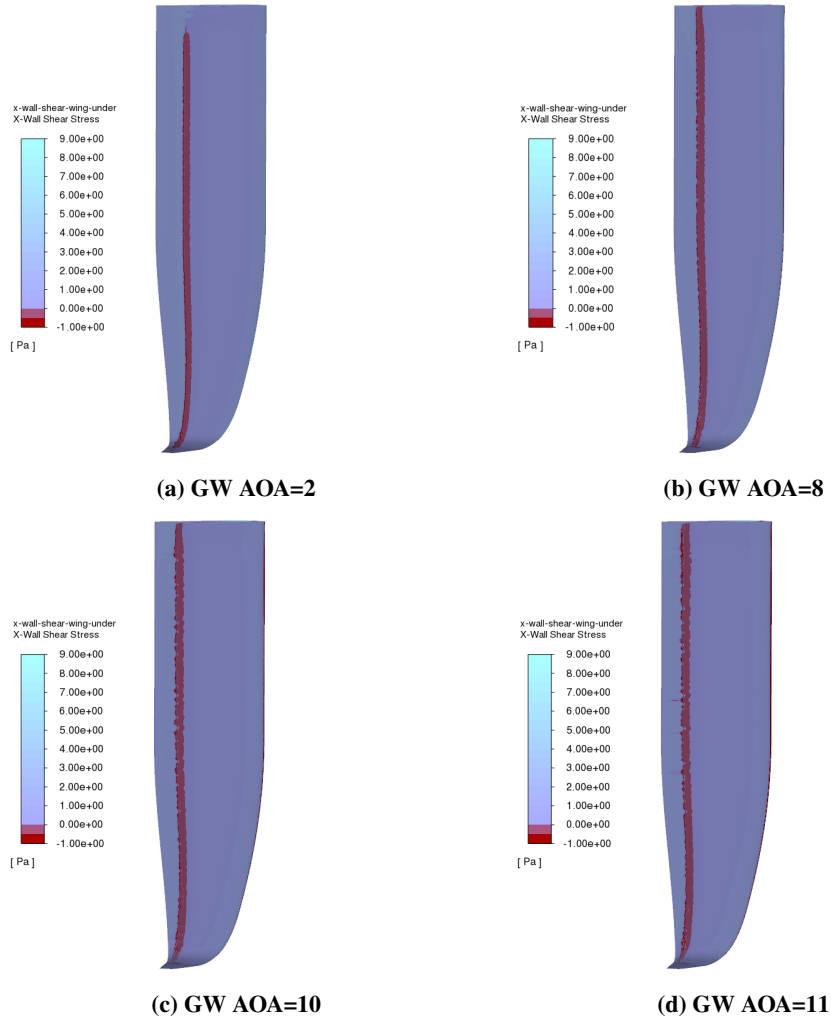

(a) GW AOA=2 **(b) GW AOA=8**

(c) GW AOA=10 **(d) GW AOA=11**

Figure 5.7: Wall shear stress in flow direction for GW on the high pressure side of the wing.

To further study the transition point cross section contours of the intermittency and velocity of the wing 2m from the center of the airplane can be seen in figure 5.8 for BW and in figure 5.9 for GW.

For BW the transition point can be seen moving forward on the low pressure side and backward on the high pressure side for GW. In figure 5.8h and 5.8g the solution did not converge and thus the results cannot be studied.

For GW the transition can be seen moving slightly forward on the low pressure side while staying roughly the same on the high pressure side. The main difference

between GW AOA 10° and GW AOA 11° is the thickness of the transition layer from laminar close to the wing and turbulent further away.

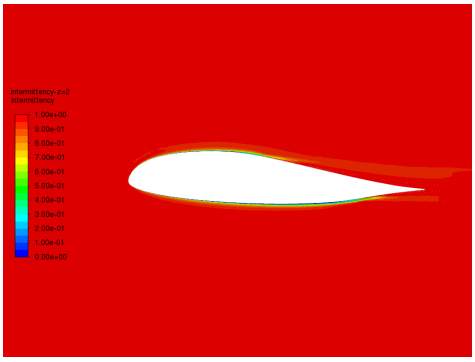

(a) BW AOA=2

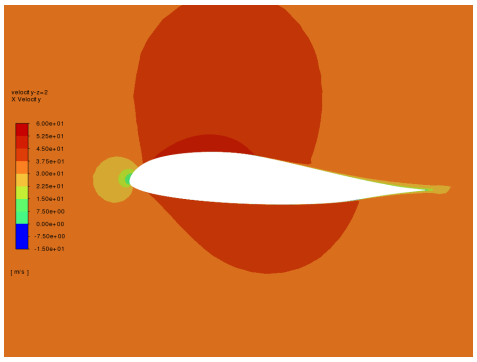

(b) BW AOA=2

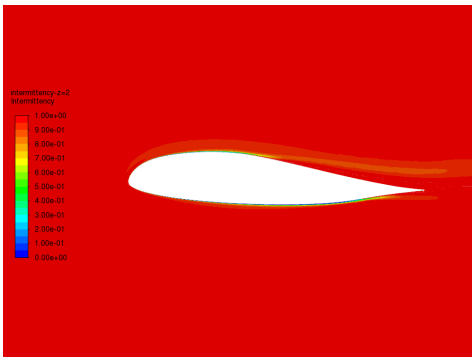

(c) BW AOA=8

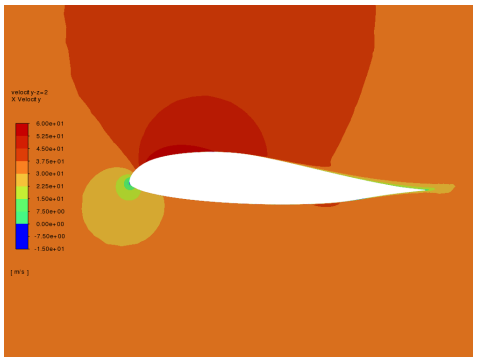

(d) BW AOA=8

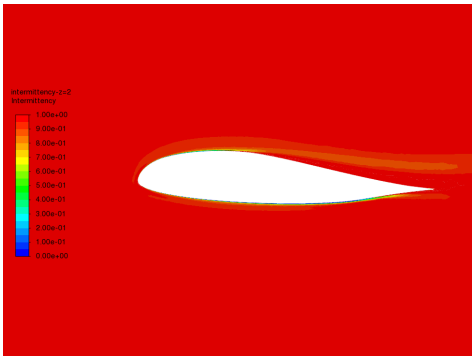

(e) BW AOA=10

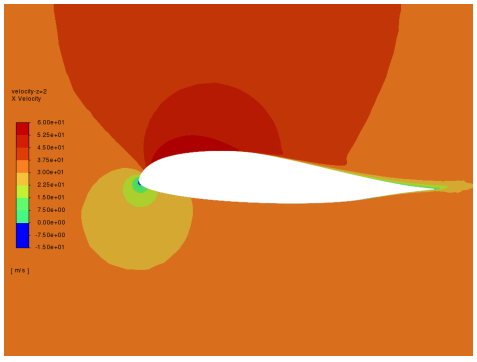

(f) BW AOA=10

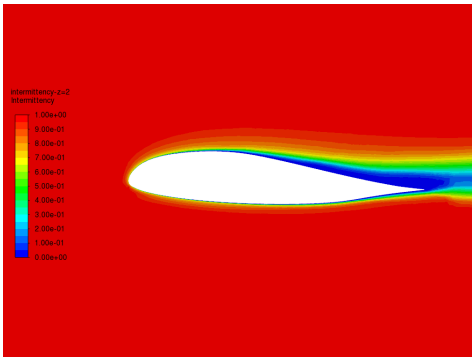

(g) BW AOA=11

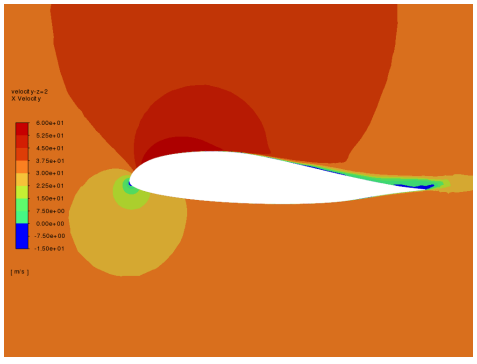

(h) BW AOA=11

Figure 5.8: Intermittency and velocity contour for BW.

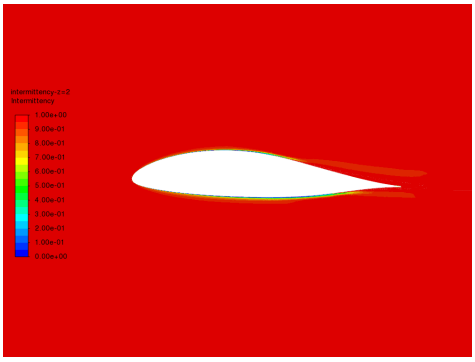

(a) GW AOA=2

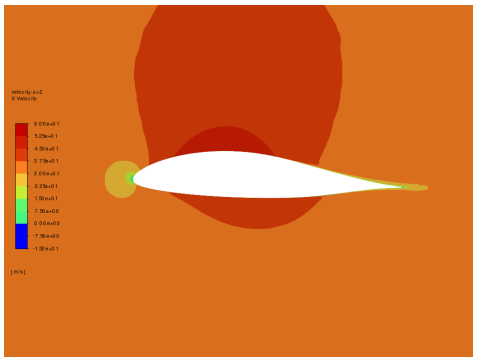

(b) GW AOA=2

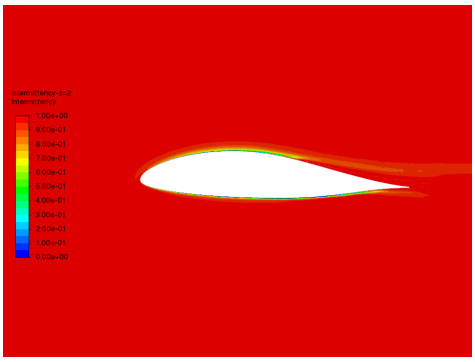

(c) GW AOA=8

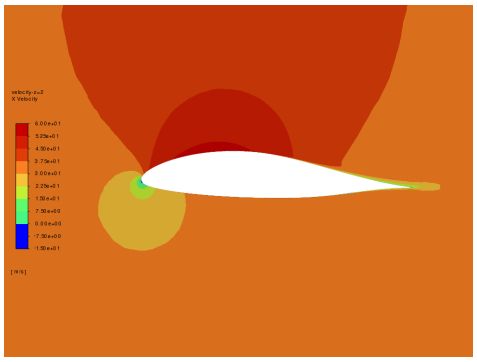

(d) GW AOA=8

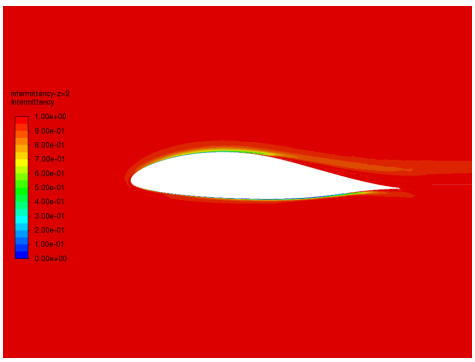

(e) GW AOA=10

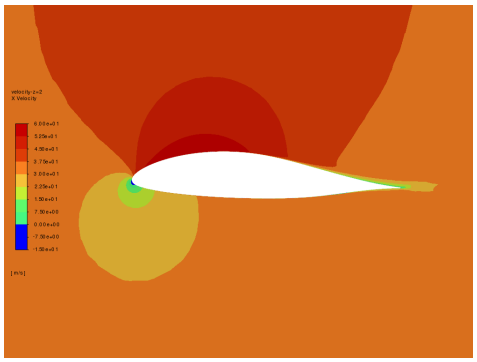

(f) GW AOA=10

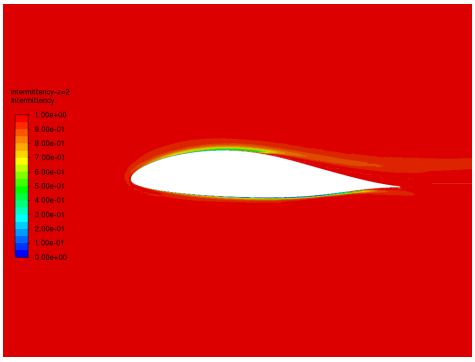

(g) GW AOA=11

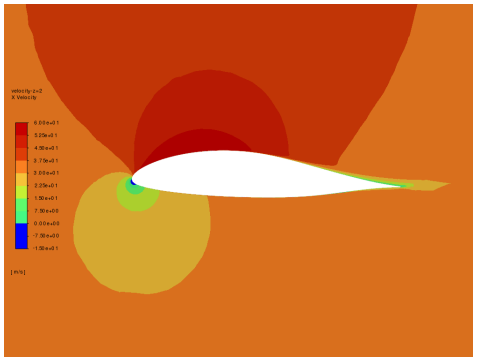

(h) GW AOA=11

Figure 5.9: Intermittency and velocity contour for GW.

5.3.2 Stall progression

As mentioned at BW AOA 11° the result did not converge, no separation can be detected before this angle thus no conclusion about the stall progression can be drawn. Most likely a time transient solver would be needed.

Separation on GW began at the root of the wing, which can be seen comparing the AOAs in figure 5.6. However, drawing conclusions on the speed of the stall progression, or investigating the appearance of the separation at critical AOAs, would require results from higher AOAs.

The overall conclusion considering stall progression is that the current model can capture when the flow will start to separate, but not how it progresses.

5.4 Efficiency

5.4.1 Results

The figure 5.10 shows the CFD results, revealing that GW has the highest C_L at higher values of C_D. At a low C_D value BW-L instead maintains C_L the longest, where GW instead rapidly drops in C_L. This trend for GW is likely due to an insufficient number of data points by the rapid drop. It can also be seen that BW and BW-L barely increase in C_L at the higher values of C_D, while GW and BW-S keep on increasing.

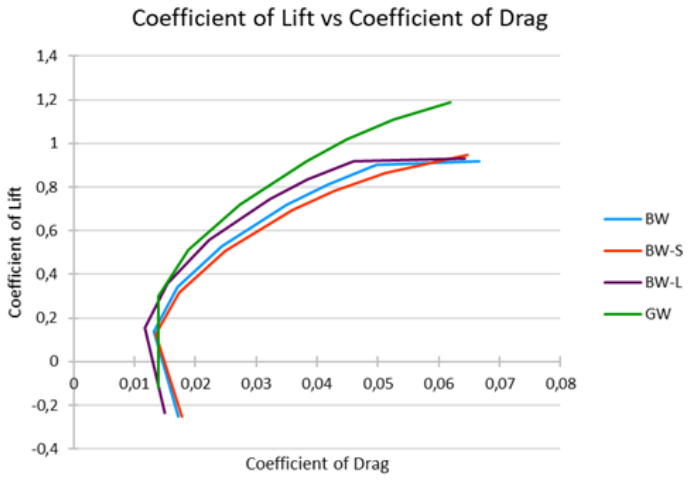

Figure 5.10: C_L **plotted against** C_D**.**

Figure 5.11 shows the Lift-to-Drag ratio versus AOA. It is clear that GW has the highest ratio for all AOAs. At lower angles of attack, i.e. around zero, the difference between GW and the BW wings is the largest. As the AOA increases, BW-L gets closer to GW and further away from BW and BW-S. Overall BW-S seem to have a lower glide ratio while behaving in a similar manner as BW.

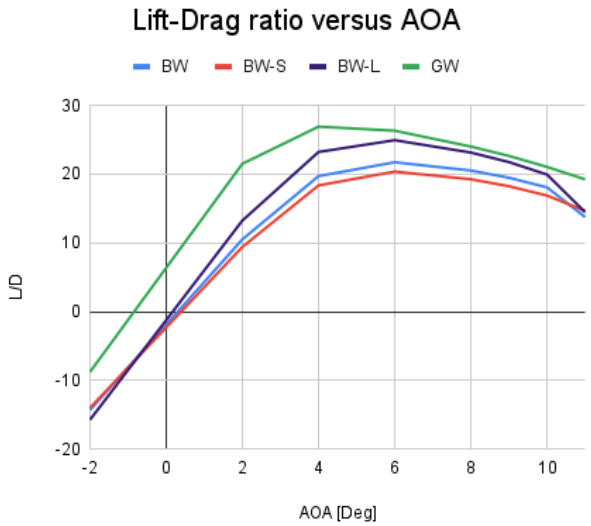

Figure 5.11: Lift-to-Drag Ratio versus angle of attack.

5.4.1.1 Drag Modelling

The CFD data points were translated into an adjusted drag model as in Equation (2.19). The adjusted drag model is plotted compared to the data in figure 5.12. A correction on the model is then made, as described in Equation (2.21). Note that the last data point from the CFD is not used in the adjusted drag model. The data point didn't fully converge and would only deteriorate the accuracy of the model. Besides, as mentioned earlier and illustrated in figure 2.6, the adjusted drag polar has issues with accuracy at higher angles of attack and would need a correction even if the data point converged.

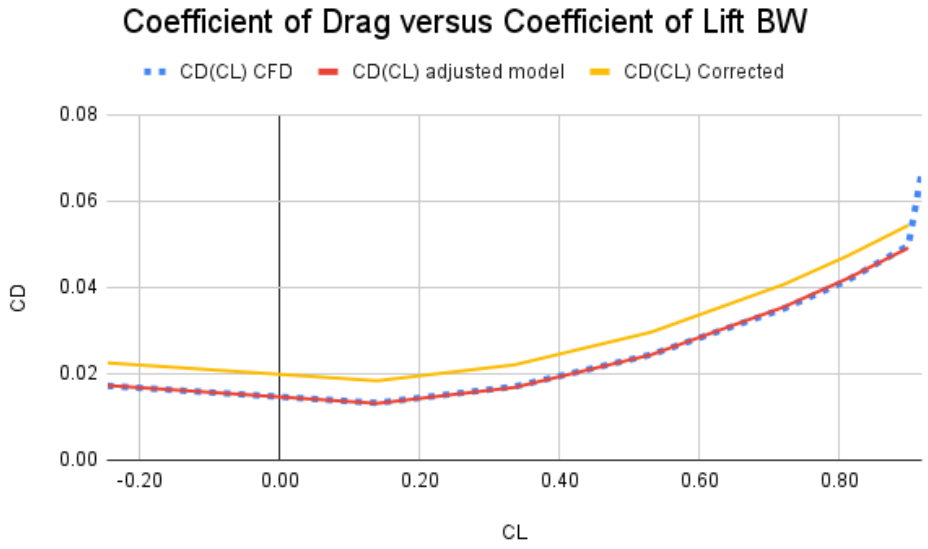

Figure 5.12: CFD, the Adjusted Drag model and the corrected Drag model for BW.

5.4.1.2 Range and Endurance

With the correction of the adjusted drag model complete for all four wings, using derivations presented earlier allowed for the estimation of D_i and D_{min} as a function of the velocity. The thrust and drag curve is presented in figure 5.13, and the required and available power is given in figure 5.14.

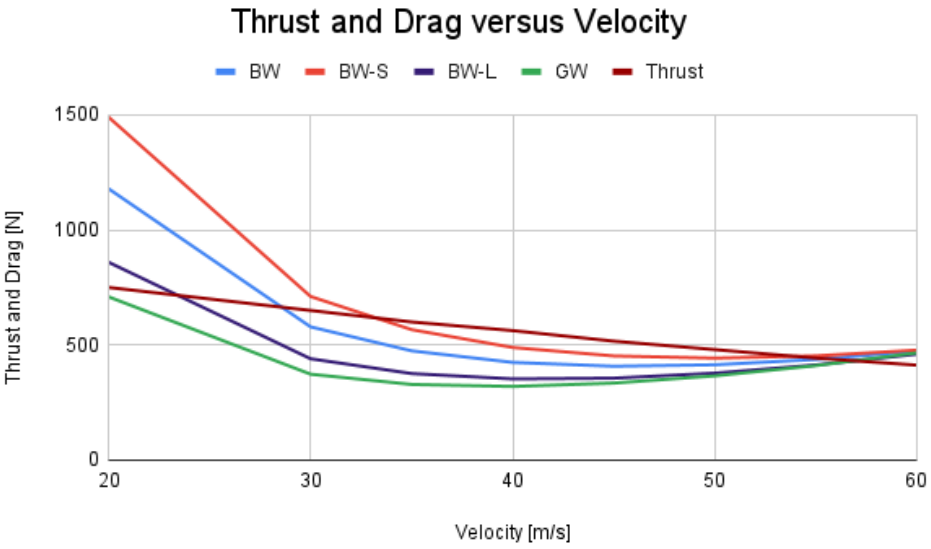

Figure 5.13: Thrust and drag forces versus the velocity, all wings compared.

From figure 5.13 it can be seen that in the region where the lift-induced drag dominates, the difference in drag between the wings is the highest. Comparing the BW wings, this implies that the longer the wing, the lower the lift-induced drag. At higher velocities, where the minimum drag is dominating, the wings total drag tend to each other.

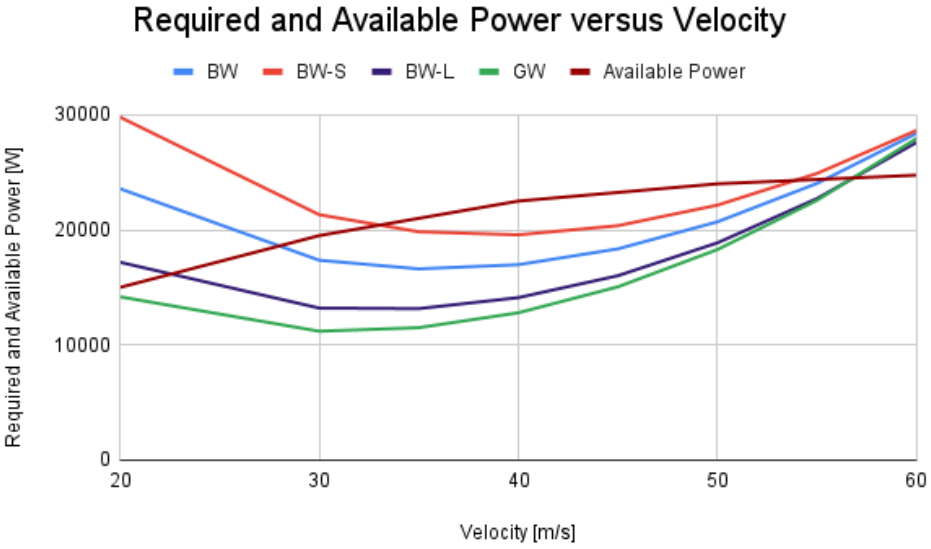

Figure 5.14: Required and available Power versus velocity, all wings compared.

The velocity at which minimum drag occurs, and the velocity at which minimum power is required can then be extracted.

A summary of the calculated parameters is given in table 5.1.

Table 5.1: Airspeeds of importance and R and E

	BW	*BW-S*	*BW-L*	*GW*
V_{min}	28.0 m/s	33.5 m/s	22.0 m/s	19.0 m/s
V_{max}	55.7 m/s	54.6 m/s	57.0 m/s	57.0 m/s
$V_{E_{max}}$	35.4 m/s	38.7 m/s	32.7 m/s	31.0 m/s
Endurance, $V_{E_{max}}$	2.1 h	1.8 h	2.6 h	3.1 h
$V_{R_{max}}$	45.4 m/s	49.7 m/s	41.7 m/s	39.1 m/s
Range, $V_{R_{max}}$	309.0 km	278.8 km	351.3 km	386.4 km
Endurance, 50 m/s	1.7 h	1.5 h	1.8 h	1.9 h

Table 5.1 show that GW has the largest velocity interval, followed by BW-L which has a higher V_{min}. BW and BW-S have a slightly lower V_{max}, and a much higher V_{min}. Note that the velocity interval is highly dependent on the available power, i.e. the thrust. The thrust curve presented here is based on the current propeller for the combustion driven aircraft. The final propeller system chosen can be tailor-made

to ensure a high efficiency at regions where it is desired, meaning these velocity intervals are not final, yet they still are of interest in comparison to each other.

The maximum endurance is achieved with GW, followed by BW-L, BW and lastly BW-S. As to maximum range, the same placement is seen. This is reasonable since the longer wings have a better glide ratio. It is also noted that, the velocities at which maximum endurance and range occur is the lowest for GW, followed by BW-L, BW and BW-S. The differences in endurance and range are significant between the wings. BW-S doesn't reach the 2 hour mark, while GW can fly over 3 hours.

The endurance at 50 m/s was calculated for all wings. The order of the placement is the same, but the difference between their endurance is lower than at their optimal velocities. If looking back at figure 5.14, it is apparent that the power required for the wings are closer at 50 m/s than when looking at their respective $V_{E_{max}}$. This comparison is important, since the maximum endurance velocities are considerably low leading to long traveling times.

5.4.2 Target Achievement

The results in table 5.1 have been calculated with a mass specific energy of 200 Wh/Kg. If plotting the endurance at 50 m/s, with a varying E^*, the endurance variation can be seen. Figure 5.15 displays this and has a 2 hour mark placed out. At 50 m/s GW and BW-L have a similar endurance, and with a E^* just over 200 Wh/Kg they reach the 2 hour target. As for BW and BW-S, they need approximately 250 Wh/Kg to reach the 2 hour target. In all of the calculations the weight of the airplane is set to the maximum allowable 750 kg in order to fit the largest amount of batteries. A weight of 600 kg is a goal for the future airplane.

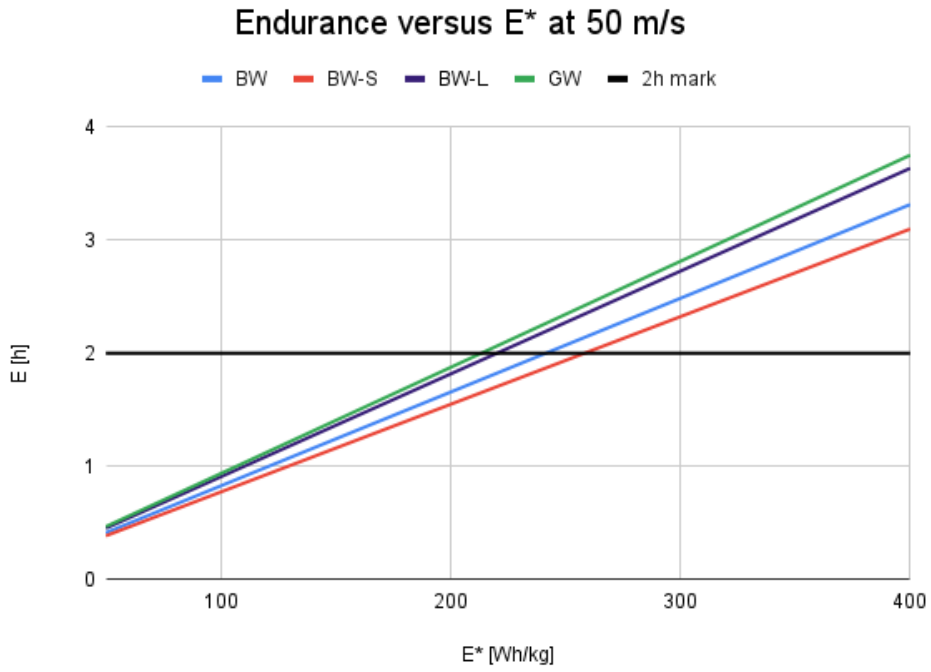

Figure 5.15: Endurance versus E^* at 50 m/s, with the 2 hour mark displayed.

5.5 Cost Aspect

In order to produce these wings, tools are needed. The cost for acquiring the new tools required to produce GW is estimated by Blackwing Sweden AB to be at least 2 million SEK. Both BW-L and BW-S would use the current tools that exist for the production of BW, thus the tooling cost would be zero. This also allows Blackwing Sweden AB to more easily build a prototype with which they can test the handling performance and compare the results to the CFD model before fully committing to the design.

5.6 Robustness of the Wing

The use of laminar airfoils require the wings to be kept clean from all contaminations such as rain and dead bugs. If the profile is not kept clean the transition point will occur at the contamination. In the case of contaminations the plane still needs to be

flyable. Since the SST k-ω model assumes a fully turbulent boundary layer it can be used to predict the behaviour of a fully contaminated wing. Recalling figure 5.3 it is noted that the BW is more robust than the GW since the difference between the turbulence models are smaller.

5.7 Wing Selection

Table 5.2 summarizes the results of the four wings, both in terms of performance and cost. The scoring range is between 0 and 1, where 1 is the highest score. The scoring is then weighted by the importance of that parameter. The importance is based on discussions with the company.

Table 5.2: Matrix scoring.

	Importance 1-5	*BW*	*BW-S*	*BW-L*	*GW*
V_{min}	2	0.68	0.57	0.86	1
V_{max}	3	0.98	0.96	1	1
Endurance, 50 m/s	5	0.89	0.79	0.95	1
Cost	4	1	1	1	0
Weighted sum	14	12.75	11.97	13.47	10

From table 5.2 the best wing design is BW-L. BW-L is therefore chosen as the wing that is the most applicable for Blackwing Sweden AB. If money wasn't of as high importance, GW would be superior, but one would need to explore the robustness of the wing in more detail.

Comparing the LD at $V_{E_{max}}$ it is noted that BW-L has a 14% higher LD than BW and GW has a 23% higher LD than BW.

5.8 Market Competitiveness

Table 5.3: Market competitiveness

	Bristell Energic	*eFlyer 2*	*BW-L*
Stall Speed	24 m/s	24 m/s	-
Max Speed	56 m/s	69 m/s	57 m/s
Endurance	1.5 h	3 h	2.6 h
Range	-	400 km	351 km
Engine Power	80 kW	100 kW	100 kW
Max take-off weight	850 kg	826 kg	750 kg

Table 5.3 shows the market competitors presented earlier, alongside with BW-L. It should be added here, that the endurance and range calculated for BW-L was done with the maximum take-off weight (in order to maintain a conservative result). A lower take-off weight would of course result in a longer range and endurance. The stall speed has not been calculated. However V_{min} reveals that the aircraft can not fly under 22 m/s.

Comparing the airplanes it would seem that BW-L is better than Bristell Energic but is outperformed by the eFlyer 2. BW-L does however have a lower weight with the same engine power and could thus have a more sporty feel. There are several more aspects to evaluate, such as the handling of the airplane, to be able to do an accurate comparison. Based on the current data available BW-L shows great potential to compete in the market. A recommendation would be to find a propeller system that allows for a higher V_{max}.

6 Conclusion

6.1 Achievement of Goals

Recalling the individual goals set at the beginning of this report to determine their fulfillment.

> 1. Model the aerodynamic performance of the existing wing and three potential wings.

The aerodynamic performance was modelled, varying AOA, for all four wings. The models were found to correspond well to each other. A difference in the separation point between the 2D and 3D case was found, however the deviation was deemed to not influence the comparison between the four wings. More potential aspects could be looked into with the current model than those that are mentioned in this report, for example the stability and structural integrity of the airplane. The differences between the wings as well as the difference that exist between the SST k-ω and the Transitional SST turbulence models are clear.

> 2. Provide a wing suggestion.

A drag model was created, allowing mapping of the performance by comparing available and required thrust, as well as the available and required power. With the endurance and range, as well as the velocity interval calculated, a wing was chosen, including the tooling cost required to produce it. GW had the best endurance, but the cost of producing the wing meant that the wing with the second best endurance, BW-L, is the final wing suggestion. The largest performance difference between the wings occurred at their respective $V_{E_{max}}$, where an increased length of the wing corresponded to a longer endurance at a lower $V_{E_{max}}$. When comparing the wings at a cruising velocity of 50 m/s the difference between the wings was decreased but the order remained unchanged.

3. Explore the achievement of the 2 h flight time target and competitiveness in the market.

The achievement of the flight target was explored and deemed not reached for the specified time and velocity of 50 m/s. By varying the specific energy of the batteries it should be achievable in a few years when the batteries capacity increases.

A comparison to other similar electrical airplanes was conducted to explore how well the airplane would be able to compete on the market. Based on the data available BW-L is a contender and taking into account the several design awards Blackwing Sweden AB have received for previous designs there should be no problem in marketing a new electric airplane.

6.2 Future Research and Investigations

When designing an airplane more aspects of the plane need to taken into account. The stability and maneuverability of the plane would need to be investigated. This could be done to a degree with the current models that exist, but the plane would need to be flown to be sure of the stability and maneuverability.

The separation that occurs when the airplane begins to stall should be explored. By using a time transient solution at higher angles of attack one would be able to investigate the separation and reattachment phenomena as well as get a better understanding of the stall progression that occurs with the aircraft.

The difference noted between the 2D and 3D case can be further investigated. If this simply is due to that cross flows aren't taken into consideration in the 2D case, this could perhaps be investigated by doing a 2.5D simulation, i.e. a cross section of the wing with a length.

A flight could be conducted using the current Blackwing and measure the required thrust at specified velocities, in order to compare it to the drag model. This would be a suitable postdiction.

In order for the airplane to be deemed airworthy a structural analysis and physical testing would need to be conducted. With a longer wing the forces that act on it are increased. A longer wing would also require a longer flap, thus increasing the requirements of the flap attachment.

An interesting aspect that could be implemented is the use of flexing or morphing composite material that would physically change the geometry of the wing at different velocities in order to achieve better properties at those velocities. Implementation

of such surfaces would require an extensive knowledge and much testing.

With electrical planes the potential design options increase. Electrical motors weigh less than combustion driven ones and thus looking into the placement of the propellers would be of interest. For example placing several across the length of the wing could increase the flight properties without adding much weight, and could be worth exploring.

Another question is how long this sort of airplane, where the engine system is changed to an electric without any other major design change, will be active on the market. Further comparison to the up and coming electrical aircraft market should be conducted. Taking a quick look into the current electrical aircraft projects that exist, this solution could be considered conventional. Will more innovative solutions that utilise the possibilities that electrical propulsion systems offer win the market over?

References

[1] Snorri Gudmundsson. *General Aviation Aircraft Design (Second Edition)*. 2nd ed. Butterworth-Heinemann, 2022. ISBN: 978-0-12-818465-3.

[2] Martin Hepperle. "Electric Flight - Potential and Limitations". In: *Energy Efficient Technologies and Concepts of Operation*. NATO Science and Technology Organization, Oct. 2012. URL: https://elib.dlr.de/78726/.

[3] Egbert Torenbeek. *Optimum cruise performance of subsonic transport aircraft*. Delft University Press, 1998. ISBN: 9040715793.

[4] Jody Muelaner. "EV battery technologies: From the state of the art to the future energy stores". In: (2022). URL: https://www.batterypowertips.com/ev-battery-technologies-from-the-state-of-the-art-to-the-future-energy-stores-faq-2/. (accessed: 13.5.2022).

[5] Frank E. Hitchens. *Propeller Aerodynamics*. Andrews UK Limited, 2015. ISBN: 978-1-78-538124-9.

[6] E.L. Houghton et al. *Aerodynamics for Engineering Students*. 7th ed. Butterworth-Heinmann, 2017. ISBN: 978-0-08-100194-3.

[7] *Forces In A Climb*. URL: https://www.grc.nasa.gov/www/k-12/airplane/climb.html. (accessed: 13.5.2022).

[8] Aerospace Engineering Blog. *Boundary Layer Separation and Pressure Drag*. 2016. URL: https://aerospaceengineeringblog.com/boundary-layer-separation-and-pressure-drag/. (accessed: 14.5.2022).

[9] L. J. Clancy. *Aerodynamics*. PITMAN PUBLISHING LIMITED, 1975.

[10] Barnaby Wainfan. *Laminar- vs. Turbulent-Flow Airfoils*. 2021. URL: https://www.kitplanes.com/laminar-vs-turbulent-flow-airfoils/#:~:text=Laminar%5C%20boundary%5C%20layers%5C%20flow%5C%20more,drag%5C%20than%5C%20turbulent%5C%2Dflow%5C%20airfoils.. (accessed: 13.5.2022).

[11] National Aeronautics and Space Administration. "Principles of Flight: Foam Wing". In: National Aeronautics and Space Administration, 2016.

[12] Gary B. Cosentino. "CFD to Flight: Some Recent Success Stories of X-plane Design to Flight Test at the NASA Dryden Flight Research Center". In: (2007).

[13] Andreas W. Schäfer et al. “Technological, economic and environmental prospects of all-electric aircraft”. In: 4 (2019), pp. 160–165.
[14] Jakub Hospodka, Helena Bínová, and Stanislav Pleninger. “Assessment of All-Electric General Aviation Aircraft”. In: (2020), pp. 2–3.
[15] *Electrical aircraft by H55 takes off for 90 minutes*. URL: https://www.electrive.com/2019/06/23/electric-aircraft-by-h55-takes-off-for-90-minutes/. (accessed: 11.5.2022).
[16] *Sun Flyer Promises Three-hour Flight Time*. URL: https://www.avweb.com/air-shows-events/sun-flyer-promises-three-hour-flight-time/. (accessed: 11.5.2022).
[17] *eFlyer 2 Electric Aircraft*. URL: https://www.aerospace-technology.com/projects/sun-flyer-2-electric-aircraft/. (accessed: 11.5.2022).
[18] *ENGINeUS™ Smart Electric Motors*. URL: https://www.safran-group.com/products-services/engineustm. (accessed: 11.5.2022).
[19] Siemens PLM Software. *Star CCM+ Documentation*. 2019.
[20] IdealSimulations Ltd. *Turbulence Models In CFD*. URL: https://www.idealsimulations.com/resources/turbulence-models-in-cfd/. (accessed: 02.1.2022).
[21] *SST k-omega model*. URL: https://www.cfd-online.com/Wiki/SST_k-omega_model. (accessed: 02.1.2022).
[22] Stephen B. Pope. *Turbulent Flows*. TJ International Ltd. Padstow Cornwall, 2000. ISBN: 9780521598866.
[23] ANSYS Inc. *ANSYS Fluent Tutorial Guide*. 2021.
[24] Tomer Avraham. *Turbulence Modeling – Near Wall Treatment*. URL: https://cfdisrael.blog/2020/05/04/sensitive-turbulence-models-near-wall-modeling-phenomenological-and-technical-explosion/. (accessed: 02.1.2022).
[25] ANSYS Inc. *Ansys Fluent Mosaic Technology Combines Disparate Meshes*. 2020.

A (Appendix)

A.1 Time plan

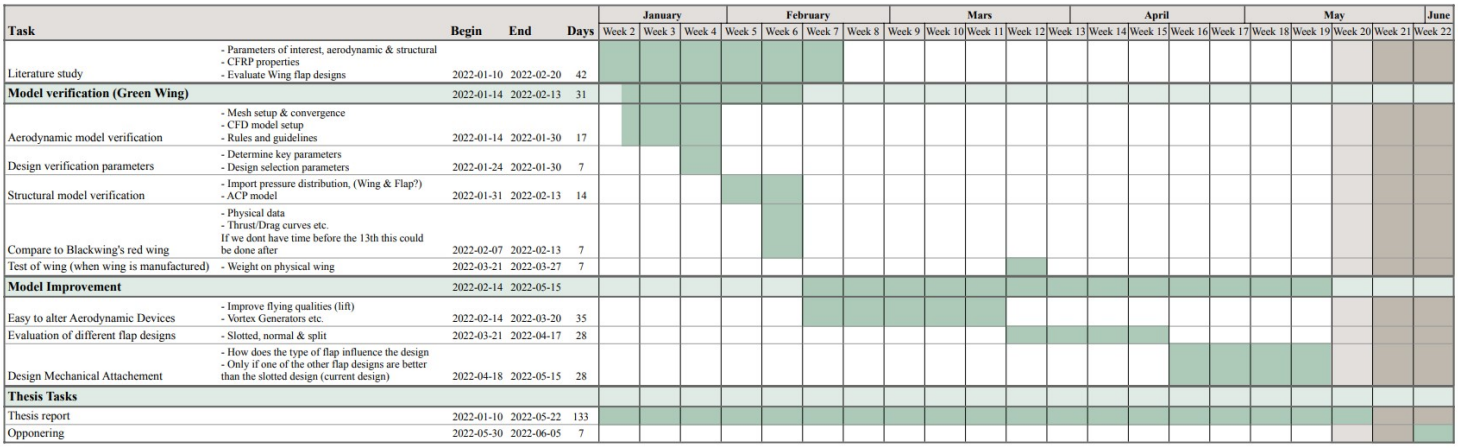

Task		Begin	End	Days
Literature study	- Parameters of interest, aerodynamic & structural - CFRP properties - Evaluate Wing flap designs	2022-01-10	2022-02-20	42
Model verification (Green Wing)		2022-01-14	2022-02-13	31
Aerodynamic model verification	- Mesh setup & convergence - CFD model setup - Rules and guidelines	2022-01-14	2022-01-30	17
Design verification parameters	- Determine key parameters - Design selection parameters	2022-01-24	2022-01-30	7
Structural model verification	- Import pressure distribution, (Wing & Flap?) - ACP model	2022-01-31	2022-02-13	14
Compare to Blackwing's red wing	- Physical data - Thrust/Drag curves etc. If we dont have time before the 13th this could be done after	2022-02-07	2022-02-13	7
Test of wing (when wing is manufactured)	- Weight on physical wing	2022-03-21	2022-03-27	7
Model Improvement		2022-02-14	2022-05-15	
Easy to alter Aerodynamic Devices	- Improve flying qualities (lift) - Vortex Generators etc.	2022-02-14	2022-03-20	35
Evaluation of different flap designs	- Slotted, normal & split	2022-03-21	2022-04-17	28
Design Mechanical Attachement	- How does the type of flap influence the design - Only if one of the other flap designs are better than the slotted design (current design)	2022-04-18	2022-05-15	28
Thesis Tasks				
Thesis report		2022-01-10	2022-05-22	133
Opponering		2022-05-30	2022-06-05	7

Figure A.1: Time plan at the initialization of the project

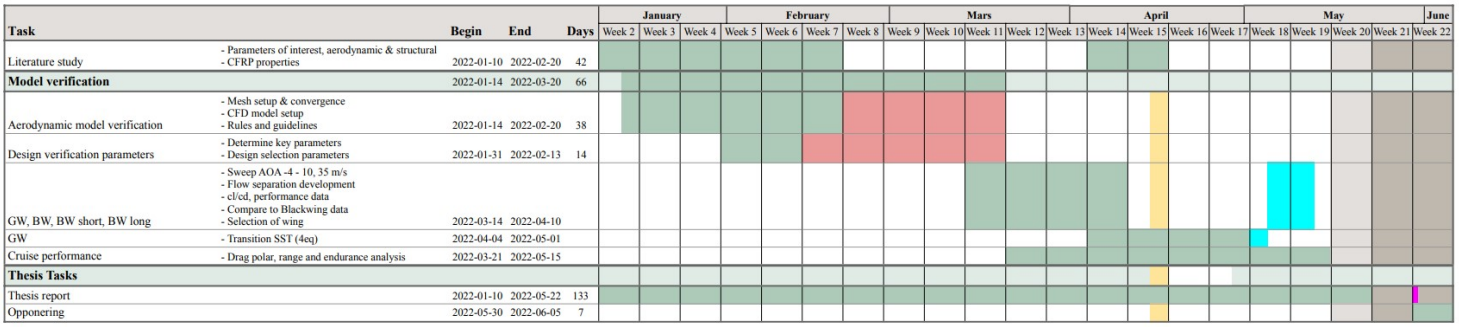

Task		Begin	End	Days
Literature study	- Parameters of interest, aerodynamic & structural - CFRP properties	2022-01-10	2022-02-20	42
Model verification		2022-01-14	2022-03-20	66
Aerodynamic model verification	- Mesh setup & convergence - CFD model setup - Rules and guidelines	2022-01-14	2022-02-20	38
Design verification parameters	- Determine key parameters - Design selection parameters	2022-01-31	2022-02-13	14
GW, BW, BW short, BW long	- Sweep AOA -4 - 10, 35 m/s - Flow separation development - cl/cd, performance data - Compare to Blackwing data - Selection of wing	2022-03-14	2022-04-10	
GW	- Transition SST (4eq)	2022-04-04	2022-05-01	
Cruise performance	- Drag polar, range and endurance analysis	2022-03-21	2022-05-15	
Thesis Tasks				
Thesis report		2022-01-10	2022-05-22	133
Opponering		2022-05-30	2022-06-05	7

Figure A.2: Time plan at the end of the project

Comparing figures A.1 and A.2 a big difference in the scope of the project can be seen. Several discussions and changes in the company's time plan affected the scope of the project which led to the projects time plan and scope altering. The main difference between the time plan occurred when a choice between either going for the first made SST $k - w$ simulations, or attempting to recreate the simulations with the Transitional SST model. The choice was to redo the simulations with the new turbulence model, the time required for the extra simulations led to the structural analysis being cut. The project therefore went from a wider scope to a more narrowed down scope, focusing on the aerodynamics and connecting it better to the literature studied. It was determined that it was more important to increase the accuracy of the results, rather than maintaining the width of the scope and the work.

A.2 Division of work

To begin with the work wasn't distributed that much between the writers. Working with aerodynamics and CFD on this level was new to both of them, and most of the early iterative work and literature study was done together. The work in design modeler (working with the domain, the bodies of influence and the aircraft model) was mainly done by Vanda, while areas such as the iterative procedure of creating the mesh and trying out settings for the turbulence models was done by both writers.

The report writing had a bit more clear division between the two writers. Vanda prepared the structure of the report as well as wrote the majority of the abstract and introduction, while Jonathan looked more into the theory focusing on the drag modelling. As for the results, Vanda focused on the results that focused on transition region and stall progression, while Jonathan put more focus on the Efficiency section. All in all, the work was done by both writers, the phase of summarizing it into a report was then just divided up based on which section they wanted to write about.